NASA TM-87620

NASA Technical Memorandum 87620

A Preliminary Evaluation Of The Generalized Likelihood Ratio For Detecting And Identifying Control Element Failures In A Transport Aircraft

W. Thomas Bundick

September 1985

NASA
National Aeronautics and
Space Administration

Langley Research Center
Hampton, Virginia 23665

SUMMARY

A failure in an aircraft control element must be accommodated in near real time by the pilot and/or automatic control system in order to prevent a possible tragic accident. A first step in this accommodation is the detection and identification of the failure. This report presents the results of an evaluation of the Generalized Likelihood Ratio (GLR) technique for the detection and identification of control element failures in transport aircraft.

The GLR technique utilizes the innovations from a Kalman Filter, which estimates the aircraft states, as inputs to the GLR algorithm. Under the assumption that the failure is a step or impulse vector function in state space, the algorithm computes the likelihood of a failure having occurred and an estimate of the failure vector. Two such algorithms, one for full GLR and one for constrained GLR, were evaluated using a digital computer linear simulation of the longitudinal dynamics of a B-737 aircraft. The full GLR algorithm assumes that the failure vector can be any vector in the state space, while the constrained GLR algorithm assumes that the failure vector is from a finite set of vectors in state space. The simulation included sensor errors and wind turbulence.

In the simulation runs all of the hard-over failures were detected by both the full GLR algorithm and the constrained GLR algorithm. Soft failures, however, were not detected with integration times up to 1.5 seconds. Results of the simulation show that while the GLR technique has potential for detecting and identifying aircraft control element failures, the effects of wind turbulence on the missed detection/false alarm performance and the effects of Kalman Filter model errors are significant problems that must be overcome.

INTRODUCTION

For certain anticipated failures in transport aircraft operations there are established procedures for the pilot to follow. A typical example is the procedure for handling an engine outage during takeoff. However, there are nearly an unlimited number of additional unanticipated failure modes for which no appropriate emergency procedures will be available. These unanticipated failures must be handled by the pilot and/or the automatic control system in real time in order to prevent a possible tragic accident.

In the case of a hard-over failure in a control element the pilot may have only a matter of seconds to take corrective action before the aircraft reaches an irrecoverable condition. In the case of a failure of lesser magnitude the pilot may have more time to take corrective action, but the failure and hence the proper corrective action may be difficult to identify. In either case the pilot may require assistance from the aircraft systems to help him take the appropriate corrective action in a timely manner.

A considerable amount of work has been done in the area of failure detection and identification (FDI) in dynamic systems, and Willsky has provided a well-known survey of many of the available FDI techniques (ref. 1). Chow (ref. 2) and Willsky and Chow (ref. 3) have examined the problem of generating residuals from the system

measurement data for use in decision making processes to detect and identify failures. The detection of failures in sensors has been investigated by several authors, including Motyka, et. al. (ref. 4), Deyst, et. al. (ref. 5), Caglayan (ref. 6), and Friedland (ref. 7). Beard (ref. 8) and Jones (ref. 9) have developed the theory behind the failure detection filter, and Messerole (ref. 10) has applied the failure detection filter to the problem of detecting and identifying failures in an F100 engine. Another FDI technique is the Generalized Likelihood Ratio (GLR). The theory of the GLR has been investigated by Willsky and Jones (ref. 11), Chow, et. al. (ref. 12), Bueno, et. al. (ref. 13), Bueno (ref. 14), MIT (ref. 15), Liu and Jones (ref. 16), and Chang and Dunn (ref. 17). The GLR technique has been developed in several versions, including full GLR, constrained GLR, and simplified GLR; these versions differ in the a priori assumptions about the type of failure. The technique has been exercised in a simplified simulation of the F-8 aircraft dynamics by Bueno and others at MIT (refs. 12-15). Tylee (ref. 18) has examined the use of the GLR to detect failures in a nuclear reactor.

This report presents the results of an evaluation of the capabilities of the full GLR and constrained GLR techniques for the detection and identification of control element failures in a transport aircraft. This evaluation was conducted primarily by implementing the GLR algorithms in a linear simulation of the longitudinal dynamics of a B-737 aircraft and examining the performance of the technique in detecting step failures in the elevator, throttle, stabilizer, or spoilers. The text includes a brief description of the GLR technique, a presentation and discussion of the results, and conclusions. The theory of the full GLR, the theory of the constrained GLR, the aircraft simulation, and the Kalman Filter are discussed in more detail in appendices A, B, C, and D, respectively.

SYMBOLS

A	system transition matrix
A_w	wind system transition matrix
A_{x_b}, A_{z_b}	acceleration in the x-, z-direction (body axes), ft/sec (sub-subscript s denotes stability axes)
B	control input matrix
B_w	wind system plant noise input matrix
b	wing span, ft
$b(\cdot)$	measurement bias error
$C(k;\theta)$	matrix defined by equations (A26) or (A45)
C_w	transformation matrix relating W to w and W_k to w_k
C_{wo}	transformation matrix C_w evaluated at $\theta = 0$
D	plant noise input matrix
D_{co}	$= D^F C^F_{wo}$

F covariance matrix of the wind system plant noise ξ

$F(k;\theta)$ matrix used in the computation of $G(k;\theta)$ and defined by equations (A35) or (A44)

f_i constrained failure vector

$G(k;\theta)$ matrix relating the innovations response $\gamma(k)$ to a failure λ and defined by equations (A34) or (A43)

$G_\bullet(s)$ filter transfer function

H observation matrix

h altitude, ft

I identity matrix

i index denoting the i-th failure vector from the set of constrained failure vectors

K Kalman Filter gain matrix

k sample number

L_u, L_w turbulence scales in the x- and z-directions, respectively, ft

$\ell(\bullet)$, $\ell(\bullet;\bullet,\bullet)$, $\ell(\bullet;\bullet,\bullet,\bullet)$ generalized log likelihood ratio, or log GLR

$P(k+1|k)$ covariance matrix of the error in the estimate $\hat{x}(k+1|k)$

$P(k|k)$ covariance matrix of the error in the estimate $\hat{x}(k|k)$

$p(\bullet|\bullet)$ conditional probability density function

Q covariance matrix of the plant noise w_k in the Kalman Filter model

q perturbed inertial pitch rate, rad/sec

q_w pitch rate due to wind, that is, rotation of the atmosphere about the y-axis, rad/sec

R covariance matrix of the observation noise v_k in the Kalman Filter model

R_ζ covariance matrix of the Kalman Filter plant disturbance ζ_F

R_η covariance matrix of the plant noise η_k

R_ξ covariance matrix of the wind system plant noise ξ_k

S_t $= \delta S$

$S_u(\bullet)$, $S_\alpha(\bullet)$, $S_q(\bullet)$ power spectral density of the x-, angle-of-attack, and pitch rate components, respectively, of the wind turbulence

t time, sec

t_k time at k-th sample, sec

U_o trim inertial velocity in x-direction, ft/sec

u, u_k control vector

$u_k(\cdot)$ components of control vector u_k

$u_s(0)$ steady state wind in the x-direction, ft/sec

u' perturbed inertial speed in the x-direction normalized by the trim velocity U_o

u'_w normalized speed in the x-direction due to wind, that is, normalized wind velocity in the negative x-direction

u'_g, u'_s gust and steady state components, respectively, of u'_w

V covariance matrix of the Kalman Filter innovations

V_a airspeed, ft/sec

v_k observation, or sensor, noise vector

W, W_k wind system state vector

$W(\cdot)$ components of wind system state vector W_k

w, w_k wind, or plant noise, vector

$w_s(0)$ steady state wind in the z-direction, ft/sec

x, x_k system state vector

$x_k(\cdot)$ component of system state vector x_k

$\hat{x}(k+1|k)$ estimate of x at time (sample number) $k+1$ given observations through time k

$\hat{x}(k|k)$ estimate of x at time (sample number) k given observations through time k

x_k Kalman Filter state vector

z, z_k observation vector

$z_k(\cdot)$ component of the observation vector z_k

α failure magnitude; perturbed inertial angle-of-attack, rad

α_w part of the angle-of-attack due to winds, rad

α_g, α_s gust and steady state components, respectively, of α_w, rad

α_o	trim value of the angle-of-attack, rad
$\gamma(k)$	vector of innovations from the Kalman Filter
$\alpha_f = \alpha$	failure magnitude
Γ	disturbance transition matrix
Γ_F	Kalman Filter disturbance transition matrix
Γ_w	disturbance transition matrix for the wind input w_k and defined by equation (C55)
δ_e	perturbed elevator position, deg
δS	perturbed stabilizer position, deg
δsp	perturbed spoiler position, deg
δst	perturbed stabilizer command, deg
δT	perturbed thrust, klbs
δth	perturbed throttle command, deg
δ_{jk}	unit step function
ζ_F	Kalman Filter plant disturbance vector
η	GLR threshold
η_k	wind disturbance vector defined by equation (C56)
θ	failure time, or sample number; perturbed pitch, rad
θ_o	trim value of pitch, rad
Λ	likelihood ratio
λ	failure vector
$\lambda(\bullet)$	components of the failure vector
ξ_k	wind system plant disturbance vector
σ_u, σ_w	RMS velocities of wind turbulence in the x- and z-directions, respectively, ft/sec
τ	time, sec
ϕ	system state transition matrix
ϕ_F	Kalman Filter state transition matrix

ϕ_W wind system state transition matrix

ψ control transition matrix

ψ_F Kalman Filter control transition matrix

Ω spatial frequency, rad/ft

ω temporal frequency, rad/sec

Notation:

~ indicates assumed value or value computed using assumed values for the independent parameters

^ indicates estimated value

F superscript F indicates that the variable is used in the Kalman Filter formulation

T superscript T denotes transpose

$E\{\cdot\}$ expectation operator

1 subscript 1 denotes that part of a vector attributed to system dynamics with no failure

2 subscript 2 denotes that part of a vector attributed to a failure

GLR TECHNIQUE

As a failure detection and identification technique the Generalized Likelihood Ratio method processes the innovations from a Kalman Filter to compute the likelihood ratio, that is, the ratio of the conditional probability of the innovations assuming a system failure has occurred to the conditional probability of the innovations assuming no failure has occurred. This ratio is then compared to a threshold value to decide whether or not the system has failed.

The GLR technique assumes that a Kalman Filter is used to track, or estimate, the states of the unfailed system, and that failures in the system are of the type that can be described as a vector in state space that occurs as an impulse or a step function at time θ. Although the technique is applicable to time-varying systems, a time-invariant formulation is used if possible to simplify the computations. Mathematically, such a system and failure are described by the state equations

$$x_{k+1} = \phi x_k + \psi u_k + \Gamma w_k + \lambda \delta_{\theta,k+1} \quad (1)$$

$$z_{k+1} = H x_{k+1} + v_{k+1} \quad (2)$$

where

x_k is the state vector

u_k is the control vector

w_k is the vector of disturbances (plant noise)

z_k is the vector of observations (measurement)

v_k is the vector of observation noise

ϕ is the state transition matrix

ψ is the control transition matrix

Γ is the disturbance transition matrix

H is the observation matrix

A failure in the system is described by the last term in equation (1), where λ is a constant failure vector which describes the magnitude and direction in state space of the failure, $\delta_{\theta,k+1}$ is a step (or impulse) function, and θ is an unknown positive integer denoting the time (sample number) of the failure.

If no failure has occurred, that is $k < \theta$, then from Kalman Filter theory the innovations from the filter are a zero mean, white, Gaussian random vector sequence. In this case the probability of occurrence of the observations is described simply by the multivariate Gaussian density with zero mean. In the case of a failure the Kalman Filter innovations are composed of a zero mean, white, Gaussian random vector sequence plus a deterministic vector sequence $G(k;\theta)\lambda$ due to the failure. In this case the probability of occurrence of the innovations is described by the multivariate Gaussian density with time-varying mean $G(k;\theta)\lambda$. The matrix sequence $G(k;\theta)$ can be computed from the state equations.

The GLR technique computes the likelihood ratio from the two probabilities just discussed and compares the ratio to the threshold to determine if a failure has occurred. The GLR algorithms also compute maximum likelihood estimates of the failure vector λ and the failure time θ.

The constrained GLR technique differs from the full GLR in the assumptions made regarding the failure vector. Whereas the full GLR allows the failure vector λ to be any vector in the state space, constrained GLR restricts the failure vector to be one of a set of vectors f_i with a scalar multiplier, or magnitude, α. This technique computes a likelihood ratio for each possible vector f_i for comparison with a threshold and computes maximum likelihood estimates of the failure magnitude α and failure time θ.

EVALUATION OF THE GLR TECHNIQUE VIA SIMULATION

The Aircraft Simulation

To achieve the objective of obtaining a preliminary evaluation of the capability of the failure detection filter to detect and identify failures in an aircraft

control system, the filter was implemented in a digital computer linear simulation of the longitudinal dynamics of a B-737 aircraft using a small perturbation model. These dynamics are described in state space by the equation

$$x_{k+1} = \phi x_k + \psi u_k + \Gamma w_k + \alpha_k f_i + \eta_k \tag{3}$$

The aircraft state vector is defined by

$$x_k = \begin{bmatrix} x_k(1) \\ x_k(2) \\ x_k(3) \\ x_k(4) \\ x_k(5) \\ x_k(6) \end{bmatrix} = \begin{bmatrix} \theta \\ u' \\ \alpha \\ q \\ \delta T \\ \delta S \end{bmatrix} \tag{4}$$

where

θ = pitch attitude

u' = normalized speed in the x-direction

α = angle-of-attack

q = pitch rate

δT = thrust

δS = stabilizer position

The control vector is defined by

$$u_k = \begin{bmatrix} u_k(1) \\ u_k(2) \\ u_k(3) \\ u_k(4) \end{bmatrix} = \begin{bmatrix} \delta_e \\ \delta th \\ \delta st \\ \delta sp \end{bmatrix} \tag{5}$$

where

δ_e = elevator command (= elevator position)

δth = throttle command

δst = stabilizer command

δsp = spoiler command (= spoiler position)

The plant noise vectors w_k and η_k represent the winds and will be discussed later. The state transition matrix ϕ, the control transition matrix ψ, and the disturbance transition matrix Γ were derived from the continuous time system matrices A, B, and D, respectively. The system matrices A, B, and D were computed from data supplied by the aircraft manufacturer for various aircraft trim conditions. All of the results discussed in this report were obtained for the aircraft trimmed for final approach on a 3 degree glideslope with the exception of a few simulation runs to evaluate the effects of modeling errors.

To evaluate the performance of the failure detection filter four types of failures with three magnitudes for each type were simulated. These four types were step failures in the elevator, throttle, stabilizer, and spoiler. The failure vectors were derived from the control transition matrix for a step change of unity magnitude, for example for an elevator position change of one degree. The three magnitudes were chosen to represent a hard-over failure, a soft failure, and a failure of intermediate magnitude. The failure types and magnitudes are listed in table I. Of course, the failure vectors change as the ψ-matrix changes with the aircraft trim conditions.

TABLE I.- FAILURE TYPES AND MAGNITUDES

Failure	
Type	Magnitude
Elevator	10°, 3°, 1°
Throttle	40°, 12°, 4°
Stabilizer	-6°, 3°, -1°
Spoiler	8°, 3°, 1°

The Wind Simulation

To provide a realistic wind environment for evaluation of the GLR technique the simulation included both turbulence, or gusts, and steady state winds. The gust components in normalized x-velocity, angle-of-attack, and pitch rate were modeled using the familiar Dryden spectra (ref. 20), which are

$$S_u(\Omega) = \frac{2\sigma_u^2 L_u}{1 + (L_u\Omega)^2} \tag{6}$$

$$S_\alpha(\Omega) = \frac{\sigma_w^2 L_w}{V_a^2} \cdot \frac{1 + 3(L_w\Omega)^2}{[1 + (L_w\Omega)^2]^2} \tag{7}$$

$$S_q(\Omega) = \frac{\Omega^2 V_a^2}{1 + (4b\Omega/\pi)^2} \cdot S_\alpha(\Omega) \tag{8}$$

where

Ω = spatial frequency, ft

b = wing span
= 93 ft

V_a = aircraft airspeed, ft/sec
= 216 ft/sec in the landing configuration simulated

L_u, L_w = turbulence scales in the x- and z-directions, respectively
= 1750 ft

σ_u, σ_w = rms velocities of turbulence in the x- and z-directions, respectively, ft/sec

After conversion from the frequency domain to the continuous time domain in state space followed by conversion to discrete time, the state equations for the wind system become

$$W_{k+1} = \phi_W W_k + \xi_k \tag{9}$$

where

W_k = 6-dimensional wind state vector with $W_k(5)$ and $W_k(6)$ being the steady state components in angle-of-attack and normalized x-velocity, respectively

ϕ_W = wind state transition matrix

ξ_k = zero mean, white, Gaussian random vector sequence

In order to provide a thorough evaluation of the GLR technique, a wide range of wind conditions were included in the simulation runs. RMS turbulence velocities corresponding to medium and heavy clear air turbulence (CAT) and to thunderstorm conditions were simulated together with steady state winds. Calm (no wind/ turbulence) conditions were also simulated. These conditions are summarized in table II.

TABLE II.- WIND CONDITIONS USED IN THE SIMULATION

Turbulence conditions	RMS gust velocity, ft/sec		Steady state wind, ft/sec	
	σ_u	σ_w	$u_s(0)$	$w_s(0)$
None	0	0	0	0
Medium	2.7	2.7	10	0
Heavy	7.0	7.0	10	0
Thunderstorm	21.0	21.0	10,39	0

The Measurements

To enhance the capability to solve the FDI problem it was desired to provide a rather complete set of measurements for input to the Kalman Filter and hence to the GLR algorithms. On the other hand, for the evaluation results to be credible, the measurement set must be technologically feasible, if not typical, for a modern day transport aircraft. The measurements selected for inclusion in the simulation are pitch attitude, x- and z-accelerations, pitch rate, airspeed, altitude rate, and angle-of-attack.

The measurements formed a 7-dimensional measurement vector z_k defined by

$$z_k = \begin{bmatrix} z_k(1) \\ z_k(2) \\ z_k(3) \\ z_k(4) \\ z_k(5) \\ z_k(6) \\ z_k(7) \end{bmatrix} = \begin{bmatrix} f_1(\theta) \\ f_2(A_{x_b}) \\ f_3(A_{z_b}) \\ f_4(q) \\ f_5(V_a) \\ f_6(\dot{h}) \\ f_7(\alpha) \end{bmatrix} \tag{10}$$

The measurements $z_k(1)$ - $z_k(7)$ include errors such as noise, bias, scale factor, and misalignment where appropriate. Numerical values for the errors are listed in table C.1.

The Filter

A 10-state Kalman Filter was used to estimate the six aircraft states and the four wind gust states and to provide the innovations for input to the GLR algorithms. For computational simplicity a constant gain filter was utilized. The measurements described in the previous paragraph were not all linear functions of the system (aircraft + wind) states as required by the Kalman Filter formulation. To circumvent this difficulty a pre-processor was used to transform the mesurement vector into a vector of pseudo-measurements, or observations, which could be approximately represented as linear functions of the system states. A more detailed description of the Kalman Filter and the pre-processor can be found in appendix D.

The time-invariant full GLR algorithms from equations (A39) through (A52) of appendix A were implemented in the simulation for evaluation. At each iteration of the simulation the algorithms computed the likelihood ratio $\ell(k;\theta)$ and the estimate $\lambda(k;\theta)$ of the failure vector for each of the windows of the most recent 2 to 30 innovations. From this set of results the algorithm computed the maximum likelihood estimates $\hat{\theta}(k)$ and $\hat{\lambda}(k)$ of the failure time and the failure vector, that is, the estimates of failure time and failure vector that corresponded to the largest likelihood ratio.

The time-invariant constrained GLR algorithms from appendix B were also implemented in the simulation for evaluation. At each iteration a series of computations similar to those for the full GLR were performed. Estimates $\hat{\alpha}$ of the failure magnitude and $\hat{\imath}$ of the failure vector index were computed rather than estimates of the failure vector.

The simulation and the GLR algorithm computations were run at a sample rate of 20 iterations per second. Because the initial interest was in detecting and identifying catastrophic type failures, a quick reaction time for the algorithm was necessary. Thus, to evaluate algorithm performance only a few seconds of flight were

required in a simulation run. With these constraints the aircraft could be flown open loop with no control system and still not diverge significantly form its nominal path before a failure was introduced. Therefore, to simplify the simulation the aircraft was flown open loop for all of the results discussed in this report.

A total of 135 simulation runs were performed to exercise the GLR technique. The results of these runs are presented and discussed in the next section.

RESULTS

Full GLR

Filter complexity and Kalman gain.- A series of 33 simulation runs were made to evaluate the performance of the GLR technique as a function of Kalman Filter complexity, or number of filter states. One of the filters was the 10-state filter described in detail in appendix D. The second filter was a 12-state filter where the two additional states were used to estimate the steady state winds. The third was a 6-state filter which estimated the aircraft states but no winds. Simulation runs were made with each filter for each of the four intermediate level failures with both medium and heavy CAT. Runs were also made with no failures introduced.

The rms estimation errors for the 10- and 12-state filters were similar, while the errors for the 6-state filter were somewhat larger. The likelihood ratios for the 10- and 12-state filters were very similar, but the GLR's for the the 6-state filter were much larger, occasionally by nearly two orders of magnitude, even for the no failure case. The larger estimation errors and the very large GLR for the no failure case relative to the GLR's for the failure cases resulted in the 6-D filter being dropped from consideration even though it was computationally simpler. The 10-D filter was chosen over the 12-D because it gave comparable performance and was slightly simpler computationally. Furthermore the 12-state system was unobservable, and some problems were experienced with matrix inversion of $C(k - \tilde{\theta})$ because C was nearly singular in some cases. The 10-state Kalman Filter and associated GLR algorithms then were used to obtain the results to be discussed in the remainder of this report.

The previous runs were made using Kalman Gains computed under the assumption of heavy turbulence ($\sigma_u = \sigma_w = 7$ ft/sec) for the filter model of plant noise. To evaluate the effect of filter gain on the performance of the GLR technique, a different matrix of Kalman gains was computed assuming thunderstorm turbulence ($\sigma_u = \sigma_w = 21$ ft/sec) for the plant noise model. Using the new gains five runs were then made simulating heavy CAT and intermediate level failures. When compared with similar previous runs using the old heavy turbulence gains, the resulting GLR's showed only slight differences. Failures were detected in three out of 12 detection possibilities with the old gains and in two out of 12 with the new gains. Differences were concluded to be insignificant, and the old heavy turbulence filter gains were used to obtain the remaining results.

Thresholds.- Three simulation runs of length 20 seconds each were made under conditions of heavy clear air turbulence ($\sigma_u = \sigma_w = 7$ ft/sec) with no failures introduced into the system. Each run was made with a different seed number for the random number generator such that each run generated a different sample function, or sequence, for the wind turbulence and for the sensor noise. From the total of these three runs the largest value computed for the likelihood ratio using a 10-sample window of data was selected for the 10-sample threshold value. Threshold values were

similarly obtained from the same runs for windows of 20 and 30 samples. Three 20 second runs were made rather than a single 60 second run because the aircraft system tended to diverge too far from the trim conditions when operating open loop for longer times.

This procedure was repeated under conditions of no turbulence to obtain a set of threshold values which could be used in evaluating the effects of wind turbulence on the performance of the GLR technique.

It was realized that this procedure would not establish a statistically reliable threshold value suitable for actual aircraft operation. However, the values thus obtained were deemed reasonable for purposes of comparing full GLR and constrained GLR performance and uncovering potential problems in using the GLR technique for aircraft control system FDI.

Failure detection performance.- Forty-six simulation runs were made to evaluate the performance of the full GLR technique under various combinations of failures, turbulence standard deviations, and steady state winds. The failures were all single point; that is, there were no multiple failures. The likelihood ratios observed for each run are shown in tables IIIa, IIIb, and IIIc for data windows of 10, 20, and 30 samples, respectively. Some of these ratios were still increasing when the simulation was terminated at 5 seconds.

These ratios were compared with the no turbulence threshold values to determine which failures were detected. The results, which are summarized in table IV, show that all failures were detected successfully with the exception of the 1 degree elevator failure which was detected in only three of the six cases. These results are very optimistic in that use of the no turbulence thresholds would produce a totally unacceptable false alarm rate. However, the results are useful when compared with later results to show the degradation in performance due to wind turbulence.

The same likelihood ratios were then compared with the thresholds obtained under conditions of heavy clear air turbulence, and the resulting detection performance is summarized in table V. Under these conditions, that is, when the threshold is set at the maximum GLR value obtained in heavy CAT with no failure, all of the hard-over failures were detected, regardless of the prevailing turbulence conditions. On the other hand, no soft failures were detected, and intermediate failures were detected in only eight of 54 opportunities. (There are three detection opportunities in each run corresponding to the three data window lengths of 10, 20, and 30 samples.) Eight of the runs were repeats of previous runs with new random noise sample functions for the turbulence and sensor noise. Examination of table III reveals how the GLR varies between the two random sample functions. From table V it can be seen that in three cases the failure was detected with one of the sample functions but not the other.

The 44 instances in which failure detection occurred (not including thunderstorms) were examined to determine the time delay between failure occurrence and failure detection, that is, the time that it took after a failure for the GLR to cross the threshold. The results, which are summarized in a histogram in figure 1, show that half of the detections occurred in less than 1 second.

Time history plots of the actual system states from the simulation and of the estimated states from the Kalman Filter are shown in figures 2(a) and 2(b) for the case of no wind turbulence and a -1 degree stabilizer failure. Since there is no turbulence and no command input, the aircraft states remain essentially unperturbed until the failure at t = 3 seconds. The action of the Kalman Filter in tracking, or

estimating, the system states can also be seen in these curves. Plots of the failure vector λ and its estimate $\hat{\lambda}$ produced by the GLR algorithm are shown in figure 2(c), and the GLR is plotted in figure 2(d). Introduction of the failure at 3 seconds does not produce a significant change in the likelihood ratio, and the GLR does not reach the threshold and hence does not detect a failure during the 5 second run. The GLR is not calculated but is set to zero during the first 2 seconds of each run to allow the filter time to settle.

Similar time history plots for the case of a -6 degree stabilizer failure with no turbulence are shown in figure 3. Note the larger perturbations in the system states for this case. In figure 3(d) the GLR is seen to cross the thresholds for the 10-, 20-, and 30-sample windows in the vicinity of 4.2 seconds and thus to declare at that point that a failure has occurred.

Time history plots for the -6 degree stabilizer failure in the presence of heavy CAT are shown in figure 4. Notice in this case the significant perturbations of the state prior to the failure and the tracking of these perturbations by the Kalman Filter. The turbulence and the filter estimate of it can be seen in figure 4(b). Once again the plot of the GLR in figure 4(d) shows detection of the failure in the vicinity of 4 seconds. Note that the curve of the 30-sample GLR is the smoothest of the three as would be expected.

Failure identification performance.- For the full GLR algorithm failure identification consists of estimating the failure vector λ. Curves of the failure vector components and their estimates for the three stabilizer failure cases in figures 2(c), 3(c), and 4(c) show step functions in the stabilizer position $\lambda(6)$ at $t = 3$ seconds, the time of the failures. The other failure vector components, $\lambda(1)$ through $\lambda(5)$, are insignificant at the scale of these curves. The estimate $\hat{\lambda}(6)$ is seen to approach the true value; however, in all three cases there are significant errors in the estimate $\hat{\lambda}(5)$. Thus it appears that there are inaccuracies in the failure identification results. There are also problems in using the failure identification information even if it were accurate; that is to say, it is not clear how an estimate $\hat{\lambda}$ of the failure vector λ would be used in restructuring the aircraft control system after a failure is declared.

Model mismatch.- The results discussed to this point were all obtained assuming a perfect knowledge of the aircraft system; that is, the aircraft model, or system matrices, used in the Kalman Filter computations was identical to the simulated aircraft. In actual practice, of course, knowledge of the system will never be perfect. To evaluate the effects of inaccuracies in the model on GLR algorithm performance, five runs were made in which the Kalman Filter model employed the same landing trim conditions used in obtaining the previous results. For the aircraft simulaton, however, take-off trim conditions were used. Model differences of this degree would be encountered if the same model were employed throughout all phases of the flight.

The likelihood ratios resulting from these runs are summarized in table VI. For each of the four failures the likelihood ratios greatly exceeded the previously established thresholds indicating failure detection. The problem, however, is that the likelihood ratios for the no failure run also greatly exceeded the threshold resulting in a false alarm. While no attempt was made to determine exactly what type or magnitude of model errors could be tolerated without serious degradation in GLR performance, this limited amount of data indicates that model inaccuracies are a potential problem with the GLR technique.

Thresholds.- Threshold values for the constrained generalized likelihood ratios (CGLR's) were found in a manner similar to those for the full GLR. Three simulation runs of length 20 seconds each were made under conditions of heavy CAT with no failures introduced into the system. The only significant difference in the procedures for the constrained GLR case and the full GLR case was that the constrained GLR algorithm for this system produced four likelihood ratios rather than one. Therefore, four thresholds were required. The three simulation runs without failures were searched to determine the largest value for each of the four CGLR's computed with a 10-sample data window. These values then were used as the 10-sample thresholds for the remaining simulation runs. Thresholds for the 20- and 30-sample data window CGLR's were similarly determined from the same runs.

Failure detection performance.- Forty simulation runs were made with various failures, turbulence levels, and steady state winds to evaluate the failure detection performance of the constrained GLR technique. The likelihood ratios from these runs were compared with the appropriate thresholds to ascertain if a failure had been detected. The results, which are summarized in table VII, show that 28 out of 40 failures were detected. Broken down by length of the data window, the results show that 24, 23, and 23 out of 40 failures were detected for the 30-, 20-, and 10-sample windows, respectively. In terms of failure magnitudes, all of the 12 hardover failures were detected, and none of the eight soft failures were detected. Of the 20 intermediate failures, 16 were detected by at least one of the data windows.

The mean detection times (time between failure and first detection) were 1.06, 0.73, and 0.53 seconds for the 30-, 20-, and 10-sample windows, respectively. A histogram of the detection times is shown in figure 5. As might be expected the 10-sample window tended to produce quicker detection because of the shorter integration time.

Time history plots for the case of a 40 degree throttle failure in the presence of heavy CAT are shown in figure 6. The true and estimated aircraft states are plotted in figure 6(a), and the increase in thrust due to the throttle failure is seen to begin at 3 seconds. In the GLR plot in figure 6(d) it can be seen that the failure is detected at approximately 3.5 seconds, or 0.5 seconds after the failure, when the GLR corresponding to a throttle failure crosses its threshold. Note that none of the other GLR's cross their respective thresholds until nearly 5 seconds.

Failure identification performance.- For the Constrained GLR algorithm failure identification consisted of estimating i, the failure vector index which defines the failure direction, and α, the failure vector magnitude. For the 70 detection opportunities in which a failure was detected successfully, the failure vector was correctly identified ($\hat{i} = i$) 52 times for an accuracy of 74 percent. These results are summarized in table VIII. Examination of these results shows that the 10-sample window did not perform as well as the 20- and 30-sample windows in identifying the failure.

Results of estimating the failure magnitude are summarized in table IX, which shows the percent error in the estimate $\hat{\alpha}$ for the cases where the failure was detected and correctly identified. The best accuracy occurred for the elevator failure, while the accuracy for the throttle failure was particularly poor.

For the 40 degree throttle failure discussed previously, examination of the estimates of the failure index and magnitude in figure 6(c) reveal that the failure

is correctly identified as soon as the failure is declared at 3.5 seconds. The estimate of the magnitude is approximately 50 degrees at the time of detection, and it improves to about 42 degrees after an additional 0.5 seconds.

Model mismatch.- Eight runs were made using a landing configuration model for the filter and a takeoff model for the simulation to assess the effects of model errors on CGLR algorithm failure detection performance. Just as was the case with the full GLR, the constrained GLR algorithm detected a failure in each of the five runs which contained a simulated failure, including one with no turbulence. However, even in the three runs with no failure introduced, including one without turbulence, one or more of the CGLR's greatly exceeded its threshold resulting in a failure false alarm. In fact, in all eight runs a failure was declared prior to 3 seconds.

CONCLUSIONS

The application of the Generalized Likelihood Ratio technique to the detection and identification of control element failures in transport aircraft has been evaluated using a linear digital simulation of a B-737 airplane. Hard-over failures in the elevator, throttle, stabilizer, and spoiler were successfully detected by both the full GLR algorithm and the constrained GLR algorithm. Some intermediate level failures were detected, but no soft failures were detected with integration times up to 1.5 seconds, that is, with data windows up to 30 samples long. One of the primary reasons for the missed detections of the lower level failures was the necessity to set the threshold level sufficiently high to avoid false alarms caused by wind turbulence. Further degradation in performance was caused by mismatch, or inaccuracies, in the Kalman Filter model.

From the results of the simulation runs, it is concluded that:

1. The GLR technique has potential application in the detection and identification of aircraft control element failures.

2. False alarms/missed detections due to wind turbulence and performance degradation due to system model inaccuracies are significant problems which must be overcome before the GLR technique can be used in a practical system.

APPENDIX A

DEVELOPMENT OF FULL GLR EQUATIONS

The development of the GLR equations in this appendix follows the development in reference 11. This appendix is included for the purpose of completeness and to include a few details not included in the reference. Furthermore, this development will be for step changes, or failures, in the system state, whereas the development in reference 11 was for impulse changes. The equations will be developed for a general, time-varying, discrete dynamic system and then constrained to a time invariant system. The application to the B-737 aircraft dynamics with its specific failures is discussed in the main body of the report and in appendix D.

The System

Consider a linear, time-varying, discrete system described by the equations

$$x(k+1) = \phi(k+1,k)x(k) + \psi(k)u(k) + \Gamma(k)\, w(k) + \lambda\delta_{\theta,k+1} \tag{A1}$$

$$z(k+1) = H(k+1)x(k+1) + v(k+1) \tag{A2}$$

where $\phi(k+1,k)$ is the state transition matrix, $\psi(k)$ is the control transition matrix, $\Gamma(k)$ is the disturbance transition matrix, $H(k+1)$ is the observation (measurement) matrix, $x(k)$ is an n-dimensional state vector, $u(k)$ is an r-dimensional command vector, $w(k)$ is an m-dimensional disturbance (plant noise) vector, $v(k+1)$ is a p-dimensional vector of sensor noise, and $z(k+1)$ is a p-dimensional observation (measurement) vector. The vectors $w(k)$ and $v(k)$ are zero mean, white, Gaussian sequences with covariance matrices $Q(k)$ and $R(k)$, respectively, that is

$$E\{w(k)\ w^T(j)\} = Q(k)\ \delta_{jk} \tag{A3}$$

$$E\{v(k)\ v^T(j)\} = R(k)\ \delta_{jk} \tag{A4}$$

where δ_{jk} is the unit impulse function.

A failure in the dynamic system is described by the last term in equation (A1), where λ is a constant n-dimensional failure vector which describes the magnitude and direction (in state space) of the failure, $\delta_{\theta,k+1}$ is a unit step function, and θ is an unknown positive integer which denotes the time (sample number) of failure.

The Kalman Filter

Now consider a Kalman Filter designed to estimate the state of the system described by equations (A1) through (A4), assuming no failures. The filter is described by

$$\hat{x}(k+1|k) = \phi(k+1,k)\hat{x}(k|k) + \psi(k)u(k) \tag{A5}$$

$$\hat{x}(k|k) = \hat{x}(k|k-1) + K(k)\ \gamma(k) \tag{A6}$$

where $\hat{x}(k|k)$ and $\hat{x}(k+1|k)$ are the estimates of the state at times k and $k+1$, respectively, given measurements up to and including time k; $\phi(k+1,k)$ and $\psi(k)$ are the state and command transition matrices, respectively; $u(k)$ is the command vector; $K(k)$ is the nxp Kalman gain matrix; and $\gamma(k)$ is the p-dimensional vector of filter innovations. The innovations are defined by

$$\gamma(k) = z(k) - H(k)\hat{x}\ (k|k-1) \tag{A7}$$

According to conventional Kalman Filter theory the variance of the innovations is given by

$$V(k) = H(k)\ P(k|k-1)\ H^T(k) + R(k) \tag{A8}$$

and the Kalman gain is given by

$$K(k) = P(k|k-1)\ H^T(k)\ V^{-1}(k) \tag{A9}$$

The estimation error covariance is propagated by the equations

$$P(k|k) = [I - K(k)\ H(k)]\ P(k|k-1) \tag{A10}$$

$$P(k+1|k) = \phi(k+1,k)P(k\ k)\phi^T(k+1,k) + \Gamma(k)Q(k)\ \Gamma^T(k) \tag{A11}$$

Response to Failure

Suppose now that a failure occurs at time θ. Since the system is linear, by the principle of superposition the system dynamic response can be separated into two parts: one part due only to the system dynamics with no failure, denoted by subscript 1, and a second part due only to the failure, denoted by subscript 2.

$$x(k) = x_1(k) + x_2(k) \tag{A12}$$

$$z(k) = z_1(k) + z_2(k) \tag{A13}$$

The response of the system to a step failure at time θ can be found by substituting equations (A12) and (A13) into equations (A1) and (A2).

$$x_2(\theta) = \lambda$$

$$x_2(\theta+1) = \phi(\theta+1,\theta)\lambda + \lambda$$

$$x_2(\theta+2) = \phi(\theta+2,\theta)\ \lambda + \phi(\theta+1,\theta)\lambda + \lambda$$

$$\vdots$$

$$x_2(k) = \sum_{j=\theta}^{k} \phi(j,\theta)\lambda \qquad k > \theta \tag{A14}$$

$$z_2(k) = H(k)x_2(k)$$

$$= H(k) \sum_{j=\theta}^{k} \phi(j,\theta)\lambda \qquad k > \theta \tag{A15}$$

In the same manner the Kalman Filter response can be separated into a part due to all effects except the failure and a part due to the effects of the failure.

$$\hat{x}(k) = \hat{x}_1(k) + \hat{x}_2(k) \tag{A16}$$

$$\gamma(k) = \gamma_1(k) + \gamma_2(k) \tag{A17}$$

The Kalman Filter response to a step failure is more tedious to develop than the system response in equations (A14) and (A15). Assume for the moment that the filter response can be expressed as

$$\hat{x}_2(k|k) = F(k;\theta)\lambda \tag{A18}$$

$$\gamma_2(k) = G(k;\theta)\lambda \tag{A19}$$

Expressions for $F(k;\theta)$ and $G(k;\theta)$ will be developed later.

The Likelihood Ratio

The problem now is to determine from an examination of the filter innovations whether or not a failure has occurred. This problem can be expressed as an hypothesis testing problem, where the hypothesis H_1 assumes a failure, that is

$$H_o: k < \theta$$

$$H_1: k \geq \theta$$

To decide between the hypotheses, form the likelihood ratio $\Lambda(k)$, that is, the ratio of the conditional probability of the occurrence of the innovation sequence $\gamma(1), \gamma(2), \ldots, \gamma(k)$ assuming H_1 to the conditional probability of occurrence of the same innovations sequence assuming H_o. The decision will be made by comparing the resulting ratio $\Lambda(k)$ to an as yet undefined threshold η.

$$\Lambda(k) \underset{H_o}{\overset{H_1}{\gtrless}} \eta \tag{A20}$$

Under the two hypotheses the filter innovations are

$$H_o: \gamma(k) = \gamma_1(k) \tag{A21}$$

$$H_1: \gamma(k) = \gamma_1(k) + G(k;\theta)\lambda \tag{A22}$$

In order to formulate the likelihood ratio, probability distributions for θ and γ must be assumed. An alternate approach is to use the generalized likelihood ratio in which the maximum likelihood estimates (MLE's) $\hat{\theta}$ and $\hat{\lambda}$ are used for θ and γ, respectively.

To find the MLE's $\hat{\theta}$ and $\hat{\lambda}$, we need the conditional probability density function for the innovations assuming H_1, $\tilde{\theta}$, and $\tilde{\lambda}$. From the theory of Kalman Filters, the innovations sequence $\gamma_1(1), \gamma_1(2), \ldots, \gamma_1(k)$ is a zero mean, white, Gaussian random vector sequence. Therefore, the sequence $\gamma(1), \gamma(2), \ldots, \gamma(k)$ is

a white, Gaussian random vector sequence with means $G(1;\theta)\lambda$, $G(2;\theta)\lambda$, ..., $G(k;\theta)\lambda$, respectively, and the corresponding conditional probability density function is

$$p[\gamma(1), \gamma(2), \ldots, \gamma(k)|H_1, \tilde{\theta}, \tilde{\lambda}]$$

$$= \prod_{j=1}^{k} \left[\frac{|V(j)|^{-1/2}}{(2\Pi)^{p/2}}\right] \exp\left\{-\sum_{j=1}^{k} [\gamma(j) - G(j;\tilde{\theta})\ \tilde{\lambda}]^T V^{-1}(j)\ [\gamma(j) - G(j;\tilde{\theta})\tilde{\lambda}]\right\} \quad \text{(A23)}$$

The MLE $\tilde{\lambda}$ assuming $\theta = \tilde{\theta}$ is found by finding the maximum of the conditional pdf. For convenience use the log pdf, and take the gradient with respect to $\tilde{\lambda}$.

$$\nabla_{\tilde{\lambda}} \left(\ell n\{p[\gamma(1), \ldots, \gamma(k)|H_1, \tilde{\theta}, \tilde{\lambda}]\}\right)$$

$$= -\sum_{j=1}^{k} [-2G^T(j;\tilde{\theta})\ V^{-1}(j)\gamma(j) + 2G^T(j;\tilde{\theta})V^{-1}(j)G(j;\tilde{\theta})\ \tilde{\lambda}] \quad \text{(A24)}$$

Let the expression in equation (A24) equal zero, and solve for $\tilde{\lambda}$.

$$\tilde{\lambda}(k;\tilde{\theta}) = C^{-1}(k;\tilde{\theta})\ d(k;\tilde{\theta}) \quad \text{(A25)}$$

where

$$C(k;\tilde{\theta}) = \sum_{j=1}^{k} G^T(j;\tilde{\theta})\ V^{-1}(j)\ G(j;\tilde{\theta}) \quad \text{(A26)}$$

$$d(k;\tilde{\theta}) = \sum_{j=1}^{k} G^T(j;\tilde{\theta})\ V^{-1}(j)\ \gamma(j) \quad \text{(A27)}$$

The conditional pdf assuming H_1 can now be rewritten as

$$p[\gamma(1),\ldots,\gamma(k)|H_1,\tilde{\theta},\tilde{\lambda}]$$

$$= \prod_{j=1}^{k}\left[\frac{|V(j)|^{-1/2}}{(2\pi)^{p/2}}\right]\exp\left\{-\sum_{j=1}^{k}\gamma^T(j)\,V^{-1}(j)\,\gamma(j)\right.$$

$$\left.+\,\tilde{\lambda}^T C(k;\tilde{\theta})\,\tilde{\lambda} - d^T(k;\tilde{\theta})\,\tilde{\lambda} - \tilde{\lambda}^T d(k;\tilde{\theta})\right\} \qquad \text{(A28)}$$

Similarly, the conditional pdf assuming H_o is

$$p[\gamma(1),\ldots,\gamma(k)|H_o]$$

$$= \prod_{j=1}^{k}\left[\frac{|V(j)|^{-1/2}}{(2\pi)^{p/2}}\right]\exp\left\{-\sum_{j=1}^{k}\gamma^T(j)\,V^{-1}(j)\,\gamma(j)\right\} \qquad \text{(A29)}$$

We are now in a position to write the generalized likelihood ratio $\Lambda(k)$, or more conveniently the log likelihood ratio $\ell(k;\tilde{\theta},\tilde{\lambda})$ as

$$\ell(k;\tilde{\theta},\tilde{\lambda}) = \ell n\left[\frac{p[\gamma(1),\ldots,\gamma(k)|H_1,\tilde{\theta},\tilde{\lambda}]}{p[\gamma(1),\ldots,\gamma(k)|H_o]}\right]$$

$$= -\tilde{\lambda}^T C(k;\tilde{\theta})\tilde{\lambda} - d^T(k;\tilde{\theta})\,\tilde{\lambda} + \tilde{\lambda}^T d(k;\tilde{\theta})$$

After substituting for $\tilde{\lambda}(k;\tilde{\theta})$ from equation (A25) the log likelihood ratio becomes

$$\ell(k;\tilde{\theta},\tilde{\lambda}) = d^T(k;\tilde{\theta})\,C^{-1}(k;\tilde{\theta})d(k;\tilde{\theta}) \qquad \text{(A30)}$$

The estimate $\tilde{\lambda}(k;\tilde{\theta})$ in equation (A25) and the likelihood ratio $\ell(k;\tilde{\theta},\tilde{\lambda})$ in equation (A30) are functions of an assumed value $\tilde{\theta}$. We must now find the MLE $\hat{\theta}$ by maximizing $\ell(k;\tilde{\theta},\tilde{\lambda})$ over $\tilde{\theta}$. This can be done by computing the estimate $\tilde{\lambda}(k;\tilde{\theta})$ and the likelihood ratio $\ell(k;\tilde{\theta},\tilde{\lambda})$ for all $\tilde{\theta}$ and choosing $\hat{\theta}(k)$ as the value of $\tilde{\theta}$ which maximizes $\ell(k;\tilde{\theta},\tilde{\lambda})$.

$$\hat{\theta}(k) = \arg\max_{\tilde{\theta}}\ \ell(k;\tilde{\theta},\tilde{\lambda}) \qquad \text{(A31)}$$

The MLE $\hat{\lambda}(k)$ and the generalized log likelihood ratio $\ell(k)$ are then

$$\hat{\lambda}(k) = \tilde{\lambda}(k;\hat{\theta}) \tag{A32}$$

$$\ell(k) = \ell(k;\hat{\theta},\hat{\lambda}) \tag{A33}$$

The GLR $\ell(k)$ in equation (A33) is compared to a threshold, as in equation (A20), to decide if a failure has occurred. If it has, then $\hat{\lambda}(k)$ and $\hat{\theta}(k)$ are the maximum likelihood estimates of the failure vector and the failure time, respectively.

Development of $F(k;\theta)$ and $G(k;\theta)$

We now need to develope algorithms for computing $F(k;\tilde{\theta})$ and $G(k;\tilde{\theta})$, which were previously used but not defined in the equations for the Kalman Filter response. Assume that the response at time $k-1$ in equations (A18) and (A19) is correct. Then the response at time k is

$$\hat{x}_2(k|k-1) = \phi(k,k-1)F(k-1;\theta)\lambda$$

$$z_2(k) = H(k) \sum_{j=\theta}^{k} \phi(j,\theta)\lambda$$

$$\gamma_2(k) = H(k) \sum_{j=\theta}^{k} \phi(j,\theta)\lambda - \phi(k,k-1)F(k-1;\theta)\lambda$$

$$= G(k;\theta)\lambda$$

$$\therefore G(k;\theta) = H(k) \sum_{j=\theta}^{k} \phi(j,\theta) - \phi(k,k-1)F(k-1;\theta) \qquad k > \theta \tag{A34}$$

$$\hat{x}_2(k|k) = \phi(k,k-1)\ F(k-1;\theta)\lambda + K(k)G(k;\theta)\lambda$$

$$\therefore F(k;\theta) = \phi(k,k-1)F(k-1;\theta) + K(k)G(k;\theta) \qquad k > \theta \tag{A35}$$

Equations (A34) and (A35) are recursive relationships for $G(k;\theta)$ and $F(k;\theta)$. A starting condition for computation can be found by considering the filter response at time $k = \theta$. A failure at time θ has no effect on the predicted response $\hat{x}(\theta|\theta-1)$. Therefore

$$\hat{x}_2(\theta|\theta-1) = 0$$

$$z_2(\theta) = H(\theta)\lambda$$

$$\gamma_2(\theta) = H(\theta)\lambda$$

$$\therefore G(\theta;\theta) = H(\theta) \qquad \text{(A36)}$$

$$\hat{x}_2(\theta|\theta) = K(\theta)H(\theta)\lambda$$

$$\therefore F(\theta;\theta) = K(\theta)H(\theta) \qquad \text{(A37)}$$

For $k < \theta$, the failure has no effect, and

$$G(k;\theta) = F(k;\theta) = 0 \qquad k < \theta \qquad \text{(A38)}$$

Time Invariant Systems

The algorithms in equations (A25) through (A27) and (A30) through (A38) constitute quite a computational workload for real time operation. This workload can be reduced significantly for the case of a time invariant system and a constant gain Kalman Filter. From equations (A34) and (A35) the filter response for this case is

$$G(k;\theta) = G(k-\theta)$$

$$= \begin{cases} 0 & k < \theta \\ H & k = \theta \\ H \sum_{j=0}^{k-\theta} \phi(j) - \phi(1)F(k-1-\theta) & k > \theta \end{cases} \qquad \text{(A39)}$$

$$F(k;\theta) = F(k-\theta)$$

$$= \begin{cases} 0 & k < \theta \\ KH & k = \theta \\ \phi(1)F(k-1-\theta) + KG(k-\theta) & k > \theta \end{cases} \qquad \text{(A40)}$$

The matrices $C(k;\tilde{\theta})$ and $d(k;\tilde{\theta})$ now become

$$C(k;\tilde{\theta}) = C(k-\tilde{\theta})$$

$$= \sum_{j=\tilde{\theta}}^{k} G^T(j-\tilde{\theta})\, V^{-1}\, G(j-\tilde{\theta}) \qquad \text{(A41)}$$

$$d(k;\tilde{\theta}) = \sum_{j=\tilde{\theta}}^{k} G^T(j-\tilde{\theta})\, V^{-1}\, \gamma(j) \qquad \text{(A42)}$$

The sequences of matrices $G(k-\tilde{\theta})$, $F(k-\tilde{\theta})$, and $C(k-\tilde{\theta})$ can all be calculated off-line and stored. The matrix sequence $d(k;\tilde{\theta})$ must be calculated in real time since it depends on the sequence of innovations.

Although the computational burden is lessened for a time invariant system, it is still formidable. The biggest reason for this is that the formulation presented above calls for the GLR and the estimates to be computed at each time k for all possible failure times $\tilde{\theta}$ from zero to the present (time k). Thus, the number of computations increases without limit as time passes. To limit the computational load the algorithms can be defined to use only a window of data at any time; that is, only the N most recent innovations $\gamma(k-N+1)$, $\gamma(k-N+2)$, ..., $\gamma(k)$ are used in the calculations. The algorithms for the off-line quantities now become

$$G(k-\tilde{\theta}) = G(n) \qquad 0 \leq n \leq N-1$$

$$= \begin{cases} H & n = 0 \\ H \sum_{j=0}^{n} \phi(j) - \phi(1)F(n-1) & n > 0 \end{cases} \qquad \text{(A43)}$$

$$F(k-\tilde{\theta}) = F(n) \qquad 0 \leq n \leq N-1$$

$$= \begin{cases} KH & n = 0 \\ \phi(1)F(n-1) + KG(n) & n > 0 \end{cases} \qquad \text{(A44)}$$

$$C(k-\tilde{\theta}) = C(n) \qquad 0 \leq n \leq N-1$$

$$= \sum_{i=o}^{n} G^T(i)\, V^{-1} G(i) \qquad \text{(A45)}$$

The computations that are done each sample time k become

$$d(k;\tilde{\theta}) = \sum_{j=\tilde{\theta}}^{k} G^T(j-\tilde{\theta})\, V^{-1}\, \gamma(j) \qquad k-N+1 \leq \tilde{\theta} \leq k \qquad \text{(A46)}$$

$$\tilde{\lambda}(k;\tilde{\theta}) = C^{-1}(k-\tilde{\theta})d(k;\tilde{\theta}) \qquad k-N+1 \leq \tilde{\theta} \leq k \qquad \text{(A47)}$$

$$\ell(k;\tilde{\theta}) = \tilde{\lambda}^T(k;\tilde{\theta})C(k-\tilde{\theta}) - d^T(k;\tilde{\theta})\, \tilde{\lambda}(k;\tilde{\theta})$$

$$- \tilde{\lambda}^T(k;\tilde{\theta})d(k;\tilde{\theta}) \qquad k-N+1 \leq \tilde{\theta} \leq k \qquad \text{(A48)}$$

$$\hat{\theta}(k) = \arg \max_{\tilde{\theta}} \ell(k;\tilde{\theta}) \qquad k-N+1 \leq \tilde{\theta} \leq k \qquad \text{(A49)}$$

$$\hat{\lambda}(k) = \tilde{\lambda}(k;\hat{\theta}) \qquad \text{A50)}$$

$$\ell(k) = \ell(k;\hat{\theta}) \qquad \text{(A51)}$$

A failure is declared if $\ell(k)$ exceeds a threshold, that is

$$\ell(k) \underset{H_0}{\overset{H_1}{>}} \eta \qquad \text{(A52)}$$

APPENDIX B

DEVELOPMENT OF ALGORITHMS FOR CONSTRAINED GLR

The development of the algorithms for constrained GLR is very similar to the development for the full GLR in appendix A. In this appendix we will concentrate on the differences between the two.

In the theory of the full GLR the failure vector λ can be any vector in the state space. However, in constrained GLR theory it is hypothesized that only a set of L failure vectors f_i are possible. Thus the state equations become

$$x(k+1) = \phi(k+1,k)x(k) + \psi(k)u(k) + \Gamma(k)w(k)$$

$$+ \alpha f_i \, \delta_{\theta,k+1} \qquad i = 1,2, \ldots, L \qquad \text{(B1)}$$

$$z(k+1) = H(k+1)x(k+1) + v(k+1) \qquad \text{(B2)}$$

where the f_i are n-vectors representing L failure directions and α is a scalar representing the failure magnitude. The other quantities are the same as for the full GLR.

Filter Response

A Kalman Filter, designed for the no-failure case, is used to estimate the system state. In the case of a step failure with failure vector f_i at time θ, the system and filter responses can again be separated into two parts: a response due to all effects other than the failure and a response due to the failure. The system response to the failure is

$$x_2(k) = \sum_{j=\theta}^{k} \phi(j,\theta) f_i \alpha \qquad \begin{matrix} i = 1, \ldots, L \\ k > \theta \end{matrix} \qquad \text{(B3)}$$

$$z_2(k) = H(k) \sum_{j=\theta}^{k} \phi(j,\theta) \, f_i \alpha \qquad \begin{matrix} i = 1, \ldots, L \\ k > \theta \end{matrix} \qquad \text{(B4)}$$

The response of the Kalman Filter to the failure is

$$\hat{x}_2(k|k) = F(k;\theta) \, f_i \alpha \qquad i = 1, \ldots, L \qquad \text{(B5)}$$

$$\gamma_2(k) = G(k;\theta) \, f_i \alpha \qquad i = 1, \ldots, L \qquad \text{(B6)}$$

where the matrices $F(k;\theta)$ and $G(k;\theta)$ are computed as in equations (A35) and (A34), respectively, of appendix A.

The conditional pdf for the innovations sequence $\gamma(1), \gamma(2), \ldots, \gamma(k)$ assuming H_1 (assuming a failure has occurred) is

$$p[\gamma(1),\ldots,\gamma(k)|H_1,\tilde{\theta},\tilde{i},\tilde{\alpha}]$$

$$= \prod_{j-1}^{k} \left[\frac{|V(j)|^{-1/2}}{(2\pi)^{p/2}}\right] \exp\left\{-\sum_{j=1}^{k} [\gamma(j) - G(j;\tilde{\theta})\, f_{\tilde{i}}\, \tilde{\alpha}]^T \right.$$

$$\left. \cdot\, V^{-1}(j)\, [\gamma(j) - G(j;\tilde{\theta})\, f_{\tilde{i}}\, \tilde{\alpha}]\right\} \qquad \text{(B7)}$$

The MLE $\tilde{\alpha}$ of the failure magnitude assumming H_1, $\tilde{\theta}$, and $\tilde{i}$ is obtained by finding the maximum of the conditional pdf.

$$\frac{\partial p}{\partial \tilde{\alpha}} [\gamma(1), \ldots, \gamma(k)|\, H_1,\tilde{\theta},\tilde{i},\tilde{\alpha}] = 0$$

Solving for $\tilde{\alpha}$ gives

$$\tilde{\alpha}(k;\tilde{\theta},\tilde{i}) = \frac{f_{\tilde{i}}^T d\,(k;\tilde{\theta})}{f_{\tilde{i}}^T C(k;\tilde{\theta})\, f_{\tilde{i}}} \qquad \text{(B8)}$$

where $C(k;\tilde{\theta})$ and $d(k;\tilde{\theta})$ are defined in equations (A26) and (A27), respectively, of appendix A.

The Likelihood Ratio

The generalized log likelihood ratio can be written as

$$\ell(k;\tilde{\theta},\tilde{i},\tilde{\alpha}) = d^T(k;\tilde{\theta})\, f_{\tilde{i}}\, \tilde{\alpha} + \tilde{\alpha}\, f_{\tilde{i}}^T d(k;\tilde{\theta}) - \tilde{\alpha}\, f_{\tilde{i}}^T C(k;\tilde{\theta})\, f_{\tilde{i}}\, \tilde{\alpha}$$

$$= \frac{d^T(k;\tilde{\theta})\, f_{\tilde{i}}\, f_{\tilde{i}}^T d\,(k;\tilde{\theta})}{f_{\tilde{i}}^T C\,(k;\tilde{\theta})\, f_{\tilde{i}}} \qquad \text{(B9)}$$

Similarly to the procedure for full GLR, the estimate $\tilde{\alpha}(k;\tilde{\theta},\tilde{i})$ and the likelihood ratio $\ell(k;\tilde{\theta},\tilde{i},\tilde{\alpha})$ are calculated for each $\tilde{i}$ and $\tilde{\theta}$, and the MLE's of θ, i, and α are those which maximize $\ell(k;\tilde{\theta},\tilde{i},\tilde{\alpha})$.

$$\hat{\theta},\hat{i} = \text{args} \max_{\tilde{\theta},\tilde{i}} \ell(k;\tilde{\theta},\tilde{i},\tilde{\alpha}) \tag{B10}$$

$$\tilde{\alpha}(k) = \alpha(k;\hat{\theta},\hat{i},) \tag{B11}$$

$$\ell(k) = \ell(k;\hat{\theta},\hat{i},\hat{\alpha}) \tag{B12}$$

Just as in the case of full GLR, the computations for the constrained GLR simplify when the system is time invariant. Similarly, the computational workload is further reduced by using only a window of the N most recent measurements. The development of the algorithms for these more restrictive cases proceeds very similarly to the development in appendix A and will not be repeated here.

APPENDIX C

SIMULATION DESCRIPTION

The Aircraft

The system used to evaluate the GLR techniques was a discrete, linear, small perturbation simulation of the longitudinal channel of a B-737 aircraft similar to the simulation described by Halyo in reference 19. Much of the development in this appendix follows that by Halyo. The discrete system was derived from a continuous time system described by the following state equations:

$$\dot{x}(t) = Ax(t) + Bu(t) + Dw(t) \tag{C1}$$

where the state vector $x(t)$ is a 6-component vector defined as

$$x(t) = \begin{bmatrix} \theta \\ u' \\ \alpha \\ q \\ \delta T \\ \delta S \end{bmatrix} \tag{C2}$$

and where the perturbed states are

θ = pitch

u' = normalized x-velocity

α = angle-of-attack

q = pitch rate

δT = thrust

δS = stabilizer deflection

The thrust and stabilizer states were included to account for the engine spool up/spool down time and for the time constant in the stabilizer actuator. The command vector $u(t)$ is defined by

$$u(t) = \begin{bmatrix} \delta e \\ \delta th \\ \delta st \\ \delta sp \end{bmatrix} \tag{C3}$$

where

δe = elevator command (= elevator position)

δth = throttle command

δst = stabilizer command

δsp = spoiler command (= spoiler position)

The wind vector is defined by

$$w(t) = \begin{bmatrix} u'_w \\ \alpha_w \\ q_w \end{bmatrix} \tag{C4}$$

where the wind components are

u'_w = normalized wind velocity in the negative x-direction

α_w = part of the angle-of-attack due to winds

q_w = rotation of the atmosphere about the y-axis

Unless otherwise specified, the quantities are defined and the equations are written in the aircraft's stability axes.

Values for the system matrices were obtained using a computer program (TCVOPL) which computes the aerodynamic coefficients for aircraft trim conditions specified by the program user. Exceptions to this procedure are the coefficients for the thrust and stabilizer states. The engine thrust is modeled as

$$\begin{aligned} \dot{\delta T} &= A_{55}\,\delta T + B_{52}\,\delta th \\ &= -0.5\ \delta T + 0.298\ \delta th \end{aligned} \tag{C5}$$

The value 0.5 was approximated from engine data for the B-737.

The response of the stabilizer on the B-737 is very slow. In order to have another control surface for restructurable controls, the time constant of the stabilizer was artificially shortened to make the surface useful. The stabilizer dynamics were assumed to be

$$\begin{aligned} \dot{\delta S} &= A_{66}\,\delta S + B_{63}\,\delta st \\ &= -0.667\ \delta S + 0.667\ \delta st \end{aligned} \tag{C6}$$

The Winds

The wind effects on the aircraft are simulated by adding them to the other aerodynamic forces acting on the aircraft. As noted in equation (C4) the wind is composed of x-velocity, angle-of-attack, and pitch rate components, and they include both steady state winds and wind gusts, or turbulence.

The gust components are modeled using the familiar Dryden spectra (ref. 20), which are defined by the following:

$$S_u(\Omega) = \frac{2\sigma_u^2 L_u}{1 + (L_u\Omega)^2} \tag{C7}$$

$$S_\alpha(\Omega) = \frac{\sigma_w^2 L_w}{V_a^2} \cdot \frac{1 + 3(L_w\Omega)^2}{\left[1 + (L_w\Omega)^2\right]^2} \tag{C8}$$

$$S_q(\Omega) = \frac{\Omega^2 V_a^2}{1 + \left(\frac{4b\Omega}{\pi}\right)^2} \cdot S_\alpha(\Omega) \tag{C9}$$

$$S_{q\alpha}(\Omega) = \frac{j\Omega}{1 + \frac{j4b\Omega}{\pi}} S_\alpha(\Omega) \tag{C10}$$

In equations (C7) through (C10) σ_u^2 and σ_w^2 are the variances of the gust velocities in the x- and z-axes, respectively, L_u and L_w are the turbulence scales in these axes, b is the aircraft wingspan, V_a is the aircraft airspeed, and Ω is the spatial frequency of the turbulence, which is related to the temporal frequency ω by

$$\omega = \Omega V_a \tag{C11}$$

In order to use these spectra in the simulation, which generates random gusts as a function of time, the spectra must be converted from functions of spatial frequency to functions of temporal frequency using the relationship

$$S(\omega) = \frac{1}{V_a} S(\omega/V_a) \tag{C12}$$

Angle-of-attack component.- Upon conversion to a function of ω the spectral density of α_g becomes

$$S_\alpha(\omega) = \frac{\sigma_w^2 L_w}{V_a^3} \cdot \frac{1 + 3(L_w/V_a)^2\omega^2}{\left[1 + (L_w/V_a)^2\omega^2\right]^2} \tag{C13}$$

which can be factored into

$$S_\alpha(\omega) = \frac{\sigma_w^2 L_w}{V_a^3} \cdot \frac{1 + j\sqrt{3}\,(L_w/V_a)\omega}{\left[1 + j(L_w/V_a)\omega\right]^2} \cdot \frac{1 - j\sqrt{3}\,(L_w/V_a)\omega}{\left[1 - j(L_w/V_a)\omega\right]^2} \tag{C14}$$

Define a transfer function $G_\alpha(s)$ using the realizable part of the spectrum in (C14).

$$G_\alpha(s) = \frac{1 + \sqrt{3}\,(L_w/V_a)s}{\left[1 + (L_w/V_a)s\right]^2} = \frac{1 + \sqrt{3}\,(L_w/V_a)s}{1 + 2(L_w/V_a)s + (L_w/V_a)^2 s^2} \tag{C15}$$

A filter with this transfer function driven by white noise with a density of $\sigma_w^2 L_w/V_a^3$ will produce random gusts with the spectral density specified by equation (C13) and with variance σ_w^2/V_a^2.

Let us now turn our attention to obtaining a set of state equations which describe the filter specified by equations (C15). First convert the transfer function to an equivalent scalar differential equation.

$$\left(\frac{L_w}{V_a}\right)^2 \ddot{\alpha}_g + \frac{2L_w}{V_a}\dot{\alpha}_g + \alpha_g = \frac{\sqrt{3}\,L_w}{V_a}\dot{\xi} + \xi$$

or

$$\ddot{\alpha}_g + \frac{2V_a}{L_w}\dot{\alpha}_g + \left(\frac{V_a}{L_w}\right)^2 \alpha_g = \frac{\sqrt{3}\,V_a}{L_w}\dot{\xi} + \left(\frac{V_a}{L_w}\right)^2 \xi \tag{C16}$$

Now let $y = -\alpha_g$ and $\xi_1 = -\xi$ in equation (C16), and let

$$W_1 = y = -\alpha_g$$

$$\dot{W}_1 = W_2 + c_1 \xi_1 \tag{C17}$$

$$\dot{W}_2 = -2(V_a/L_w)W_2 - (V_a/L_w)^2 W_1 + c_2 \xi_1$$

From equations (C17) find expressions for $\dot{y}$ and $\ddot{y}$.

$$\dot{y} = W_2 + c_1 \xi_1$$

$$\ddot{y} = -2(V_a/L_w)W_2 - (V_a/L_w)^2 W_1 + c_2 \xi_1 + c_1 \dot{\xi}_1 \tag{C18}$$

Substitute these in equation (C16), and solve for c_1 and c_2.

$$c_1 = \sqrt{3}\ (V_a/L_w)$$

$$c_2 = (1 - \sqrt{12})(V_a/L_w)^2 \tag{C19}$$

Pitch component.- Upon conversion to a function of ω the power spectral density of the pitch gusts becomes

$$S_q(\omega) = \frac{\omega^2}{1 + (4b/\pi V_a)^2 \omega^2} S_\alpha(\omega)$$

$$= \frac{j\omega}{1 + j(4b/\pi V_a)\omega} G_\alpha(j\omega) \cdot \frac{-j\omega}{1 - j(4b/\pi V_a)\omega} G_\alpha(-j\omega) \tag{C20}$$

The wind gusts in pitch can be simulated by passing angle-of-attack gusts, that is the output of the filter $G_\alpha(s)$, through a filter with a transfer function $G_q(s)$ defined by

$$G_q(s) = \frac{s}{1 + (4b/\pi V_a)s} \tag{C21}$$

To obtain a state variable representation of the filter, first find the scalar differential equation equivalent of the transfer function $G_q(s)$.

$$\frac{4b}{\pi V_a}\dot{q}_g + q_g = \dot{\alpha}_g = -\dot{w}_1 \tag{C22}$$

Let

$$q_g = -\frac{\pi V_a}{4b} w_1 + \frac{\pi V_a}{4b} w_3 \tag{C23}$$

Then

$$-\dot{w}_1 + \dot{w}_3 - \frac{\pi V_a}{4b} w_1 + \frac{\pi V_a}{4b} w_3 = -\dot{w}_1 \tag{C24}$$

Therefore

$$\dot{w}_3 = \frac{\pi V_a}{4b} w_1 - \frac{\pi V_a}{4b} w_3 \tag{C25}$$

X-axis component.- Upon conversion to a function of ω the power spectral for the gusts along the x-axis becomes

$$S_u(\omega) = \frac{2L_u\sigma_u^2}{V_a^3} \cdot \frac{1}{1 + (L_u/V_a)^2\omega^2} \tag{C26}$$

$$= \frac{2L_u\sigma_u^2}{V_a^3} \cdot \frac{1}{1 + j(L_u/V_a)\omega} \cdot \frac{1}{1 - j(L_u/V_a)\omega}$$

The x-axis gusts can be obtained by passing white noise with density $2L_u\sigma_u^2/V_a^3$ through a filter with transfer function $G_u(s)$ defined by

$$G_u(s) = \frac{1}{1 + (L_u/V_a)s} \tag{C27}$$

The corresponding scalar differential equation is

$$\frac{L_u}{V_a}\dot{u}'_g + u'_g = \xi_2 \tag{C28}$$

or in terms of state variables

$$\begin{aligned} W_4 &= u'_g \\ \dot{W}_4 &= -\frac{V_a}{L_u}W_4 + \frac{V_a}{L_u}\xi_2 \end{aligned} \tag{C29}$$

Steady state winds.- The steady state winds have an x-axis component and an angle-of-attack component each of which is simulated as the output of a first order differential equation driven by white noise with a very small variance. This allows the winds to vary slightly during a run. The desired steady state wind velocities are used as the initial conditions. Mathematically the winds are described as follows:

$$\begin{aligned} \dot{u}'_s(t) &= \xi_3; \qquad u'_s(0) = u_s(0)/U_o \\ \dot{\alpha}_s(t) &= \xi_4; \qquad \alpha_s(0) = w_s(0)/U_o \end{aligned} \tag{C30}$$

Wind state equations.- Equations (C17), (C25), (C29), and (C30) can be combined to describe the total winds as follows:

$$\dot{W} = A_W W + B_W \xi \tag{C31}$$

where

$$W = \begin{bmatrix} w_1 \\ w_2 \\ w_3 \\ w_4 \\ w_5 \\ w_6 \end{bmatrix}$$

$$A_W = \begin{bmatrix} 0 & 1 & 0 & 0 & 0 & 0 \\ -(V_a^2/L_w^2) & -(2V_a/L_w) & 0 & 0 & 0 & 0 \\ (\pi V_a/4_b) & 0 & -(\pi V_a/4_b) & 0 & 0 & 0 \\ 0 & 0 & 0 & -(V_a/L_u) & 0 & 0 \\ 0 & 0 & 0 & 0 & 0 & 0 \\ 0 & 0 & 0 & 0 & 0 & 0 \end{bmatrix} \qquad \text{(C32)}$$

$$\xi = \begin{bmatrix} \xi_1 \\ \xi_2 \\ \xi_3 \\ \xi_4 \end{bmatrix} \qquad \text{(C33)}$$

$$B_W = \begin{bmatrix} (\sqrt{3}\ V_a/L_w) & 0 & 0 & 0 \\ (1 - \sqrt{12}) \cdot (V_a/L_w) & 0 & 0 & 0 \\ 0 & 0 & 0 & 0 \\ 0 & (V_a/L_u) & 0 & 0 \\ 0 & 0 & 1 & 0 \\ 0 & 0 & 0 & 1 \end{bmatrix} \qquad \text{(C34)}$$

The covariance matrix of the Gaussian vector ξ is

$$F = E\{\xi\xi^T\}$$

$$F = \begin{bmatrix} (\sigma_w^2 L_w/V_a^3) & 0 & 0 & 0 \\ 0 & (2L_u\sigma_u^2/V_a^3) & 0 & 0 \\ 0 & 0 & 1/V_a^3 & 0 \\ 0 & 0 & 0 & 1/V_a^3 \end{bmatrix} \tag{C35}$$

In the foregoing formulation the wind gusts W_1 through W_4 were written in aircraft body axes, and the steady state winds W_5 and W_6 were written in earth axes. They must be transformed into stability axes. Furthermore, the gust and steady state components must be added, and W_1 and W_3 must be combined according to equation (C2) in order to obtain proper wind forces acting on the aircraft. This can all be accomplished with the transformation C_W as follows:

$$w = C_W W \tag{C36}$$

where

$$w = \begin{bmatrix} w_1 \\ w_2 \\ w_3 \end{bmatrix} = \begin{bmatrix} u_w' \\ \alpha_w \\ q_w \end{bmatrix} = \begin{bmatrix} u_g' + u_s' \\ \alpha_g + \alpha_s \\ q_g \end{bmatrix} \tag{C37}$$

and

$$C_W = \begin{bmatrix} -\sin\alpha_o & 0 & 0 & -\cos\alpha_o & -\cos(\theta_o - \alpha_o + \theta) & \sin(\theta_o - \alpha_o + \theta) \\ -\cos\alpha_o & 0 & 0 & \sin\alpha_o & -\sin(\theta_o - \alpha_o + \theta) & -\cos(\theta_o - \alpha_o + \theta) \\ -(\pi V_a/4b) & 0 & (\pi V_a/4b) & 0 & 0 & 0 \end{bmatrix} \tag{C38}$$

Discrete State Equations

The state equations for the aircraft and winds have been written as functions of continuous time t. These equations need to be coverted to functions of discrete time t_k for use in a digital computer simulation. Such a discretization has been discussed by Halyo (ref. 19).

Consider the aircraft continuous time state equation (C1). If the state is known at time t_k, the state at time $t_{k+1} = t_k + T$ can be found by integration over the interval t_k to t_{k+1}. The result is shown in many texts (e.g., ref. 21) to be

$$x(t_{k+1}) = \phi(t_{k+1}, t_k)x(t_k) + \int_{t_k}^{t_{k+1}} \phi(t_{k+1}, \tau)Bu(\tau)\, d\tau$$

$$+ \int_{t_k}^{t_{k+1}} \phi(t_{k+1}, \tau)Dw(\tau)\, d\tau \qquad \text{(C39)}$$

where

$$\phi(t, \tau) = e^{A(t-\tau)}$$

To simplify the notation, let $x(t_k)$ be denoted by x_k, and assume that the command $u(t)$ is constant over the integral $t_k \leq t < t_{k+1}$. Then

$$x_{k+1} = \phi(k+1, k)x_k + \int_{t_k}^{t_{k+1}} \phi(t_{k+1}, \tau)\, d\tau\, Bu_k$$

$$+ \int_{t_k}^{t_{k+1}} \phi(t_{k+1}, \tau)Dw(\tau)\, d\tau \qquad \text{(C40)}$$

The integral $\int_{t_k}^{t_{k+1}} \phi(t_{k+1}, \tau)\, d\tau$ can be expressed as

$$\int_{t_k}^{t_{k+1}} e^{A(t_{k+1}-\tau)}\, d\tau\, B = e^{At_{k+1}} \int_{t_k}^{t_{k+1}} e^{-A\tau}\, d\tau\, B \qquad \text{(C41)}$$

If A has an inverse A^{-1}, then

$$\psi = \int_{t_k}^{t_{k+1}} e^{A(t_{k+1}-\tau)}\, d\tau\, B = e^{At_{k+1}} \int_{t_k}^{t_{k+1}} e^{-At} A^{-1}\, d(A\tau)B$$

$$= e^{At_{k+1}} \left[-e^{-At_{k+1}} + e^{-At_k} \right] A^{-1}B \qquad \text{(C42)}$$

$$= [\phi(k+1,k) - I]A^{-1}B$$

The aircraft state equation now becomes

$$x_{k+1} = \phi x_k + \psi u_k + \int_{t_k}^{t_{k+1}} \phi(t_{k+1}, \tau) Dw(\tau)\, d\tau \qquad \text{(C43)}$$

To evaluate the integral involving the wind $w(\tau)$, we first convert the continuous time wind state equation (C31) to discrete time.

$$\dot{W} = A_W W + B_W \xi \qquad \text{(C31)}$$

Upon integration this becomes

$$W_{k+1} = \phi_W W_k + \xi_k \qquad \text{(C44)}$$

where ϕ_W is the state transition matrix for the wind system.

$$\phi_W = \phi_W(k+1, k)$$

$$= e^{A_W(t_{k+1}-t_k)} \qquad \text{(C45)}$$

and

$$\xi_k = \int_{t_k}^{t_{k+1}} \phi_w(t_{k+1}, \tau) B_w \xi(\tau)\, d\tau$$

$$= \int_0^T \phi_w(T, \tau) B_w \xi(t_k + \tau)\, d\tau \qquad \text{(C46)}$$

Halyo (ref. 19) has shown that ξ_k is a Gaussian white noise vector sequence with covariance R_ξ.

$$R_\xi(k,j) = E\{\xi_k \xi_j^T\}$$

$$= E\left\{ \int_0^T \phi_w(T, \tau) B_w \xi(t_k + \tau)\, d\tau \cdot \int_0^T \xi^T(t_j + s) B_w^T \phi_w^T(T, s)\, ds \right\} \qquad \text{(C47)}$$

$$= \int_0^T \int_0^T \phi_w(T, \tau) B_w E\{\xi(t_k + \tau)\xi^T(t_j + s)\} B_w^T \phi_w^T(T, s)\, d\tau\, ds$$

Since $\xi(t)$ is a white noise process, and since the intervals $(t_k, t_k + T)$ and $(t_j, t_j + T)$ do not overlap for $j \neq k$,

$$E\{\xi(t_k + \tau)\xi^T(t_j + s)\} = \begin{cases} 0 & j \neq k \\ F\delta(\tau - s) & j = k \end{cases} \qquad \text{(C48)}$$

Therefore,

$$R_\xi(k,j) = R_\xi \delta_{jk} \qquad \text{(C49)}$$

$$R_\xi = \int_0^T \phi_w(T, s) B_w F B_w^T \phi_w(T, s)\, ds \qquad \text{(C50)}$$

The matrix C_W, which transforms the continuous time wind variables W into the variables w for use as the plant noise in the aircraft state equations, is still valid for the discrete case. Thus

$$w_k = C_W W_k \tag{C51}$$

We now return to the evaluation of the integral in equation (C43) involving the wind $w(\tau)$. A change of variables produces

$$\int_{t_k}^{t_{k+1}} \phi(t_{k+1}, \tau) Dw(\tau)\, d\tau = \int_0^T \phi(T,s) Dw(t_k + s)\, ds \tag{C52}$$

After substitution of equation (C36), integration of equation (C44) from 0 to T, and substitution of equation (C46), the integral becomes

$$\int_0^T \phi(T,s) Dw(t_k + s)\, ds = \int_0^T \phi(T,s) DC_W \phi_W(s,0)\, ds\, W_k + \int_0^T \phi(T,s) DC_W \int_0^s \phi_W(s,\tau) B_W \xi(t_k + \tau)\, d\tau\, ds \tag{C53}$$

The aircraft state equation can now be written as

$$x_{k+1} = \phi x_k + \psi u_k + \Gamma_W W_k + \eta_k \tag{C54}$$

where

$$\Gamma_W = \int_0^T \phi(T,s) DC_W \phi_W(s,0)\, ds \tag{C55}$$

and

$$\eta_k = \int_0^T \phi(T,s) DC_W \int_0^s \phi_W(s,\tau) B_W \xi(t_k + \tau)\, d\tau\, ds \tag{C56}$$

The sequence η_k is a Gaussian white noise vector sequence with covariance R_η.

$$R_\eta(k,j) = E\{\eta_k \eta_j^T\}$$

$$= \int_0^T \int_\tau^T \phi(T,s)DC_W\phi_W(s,\tau)\, ds\, B_W\xi(t_k + \tau)\, d\tau$$

$$\cdot \int_0^T \xi(t_j + y)B_W^T \int_y^T \phi_W^T(x,y)C_W^T\phi^T(T,x)\, dx\, dy \qquad \text{(C57)}$$

$$= \int_0^T \int_0^T \int_\tau^T \phi(T,s)DC_W\phi_W(s,\tau)\, ds\, B_W E\{\xi(t_k + \tau)\xi^T(t_j + y)\}$$

$$\cdot B_W^T \int_y^T \phi_W^T(x,y)C_W^T D^T\phi^T(T,x)\, dx\, dy\, d\tau$$

As we noted previously in equation (C48),

$$E\{\xi(t_k + \tau)\xi^T(t_j + y)\} = \begin{cases} 0 & j \neq k \\ F\delta(\tau - y) & j = k \end{cases} \qquad \text{(C58)}$$

Therefore

$$R_\eta(j,k) = R_\eta\delta_{jk} \qquad \text{(C59)}$$

$$R_\eta = \int_0^T \left[\int_\tau^T \phi(T,s)DC_W\phi_W(s,\tau)\, ds\right] B_W F B_W^T$$

$$\cdot \left[\int_\tau^T \phi_W^T(x,\tau)C_W^T D^T\phi^T(T,x)\, dx\right] d\tau \qquad \text{(C60)}$$

This completes the discretization of the state equations necessary to simulate the aircraft and winds.

Measurements

Thus far we have described the simulation of the aircraft dynamics and of the winds acting on the aircraft. For the purposes of the work discussed in this report the simulation needs one additional element - simulation of the measurements, or aircraft sensor outputs.

The measurements of interest are pitch attitude from a pitch gyro, x- and z-accelerations from body mounted accelerometers, pitch rate from a pitch rate gyro, airspeed and altitude rate from the air data computer, and angle-of-attack from an angle-of-attack vane. A reasonably accurate simulation requires computation of the true value of the quantity being measured and then the addition of appropriate errors. For each measurement these errors include some, but not necessarily all, of the following: bias, white noise, scale factor, and alignment. The true values and errors are combined at each sample time t_k to form a measurement vector z_k.

$$z_k = \begin{bmatrix} z_k(1) \\ z_k(2) \\ \vdots \\ z_k(7) \end{bmatrix} \tag{C61}$$

Pitch.- The pitch measurement includes additive noise and bias errors.

$$z_k(1) = \theta + v_k(1) + b(1) \tag{C62}$$

where

θ = pitch = $x_k(1)$

$b(1) = 0.23°$

$v_k(1)$ = zero mean white Gaussian noise

$E\{v_k^2(1)\} = (0.23°)^2$

Accelerations.- The x- and z-axis acceleration measurements include noise, bias, scale factor, and misalignment errors. The first step in obtaining a simulated measurement is to compute the true value of the acceleration in stability coordinates, A_{x_s} and A_{z_s}, from the equations of motion.

$$A_{x_s} = U_o\dot{u}' + qU_o \tan \alpha + g \sin(\theta_o + \theta - \alpha_o)$$

$$A_{z_s} = U_o[\dot{u}' \tan \alpha + (1 + u')\dot{\alpha}/\cos^2 \alpha] - qU_o - g \cos(\theta_o + \theta - \alpha_o) \qquad \text{(C63)}$$

where

g = acceleration due to gravity

U_o = trim inertial velocity along x

θ_o = trim pitch attitude

α_o = trim angle-of-attack

θ = perturbed pitch = $x_k(1)$

u' = perturbed inertial velocity along x = $x_k(2)$

α = perturbed inertial angle of attack = $x_k(3)$

q = perturbed pitch rate = $x_k(4)$

At any time t_k values of x_k are known from the aircraft state equation. The quantities $\dot{u}'$ and $\dot{\alpha}$ are calculated using the coefficients from the continuous time state equation.

$$\left.\begin{aligned} \dot{u}' &= \varepsilon_2^T[Ax_k + Bu_k + Dw_k] \\ \dot{\alpha} &= \varepsilon_3^T[Ax_k + Bu_k + Dw_k] \end{aligned}\right\} \qquad \text{(C64)}$$

where

$$\varepsilon_2^T = [0\ 1\ 0\ 0\ 0\ 0]$$

$$\varepsilon_3^T = [0\ 0\ 1\ 0\ 0\ 0]$$

These stability axis accelerations are transformed into body axis accelerations, and the effects of accelerometer misalignment are added as follows:

$$\left.\begin{aligned} A_{x_b} &= A_{x_s} \cos(\alpha_o + a) - A_{z_s} \sin(\alpha_o + a) \\ A_{z_b} &= A_{x_s} \sin(\alpha_o + a) + A_{z_s} \cos(\alpha_o + a) \end{aligned}\right\} \quad \text{(C65)}$$

where

a = accelerometer alignment error = 0.2°

Noise, bias, and scale factor errors are added to obtain the acceleration measurements.

$$\left.\begin{aligned} z_k(2) &= \left[A_{x_b} + v_k(2) + b(2)\right] \cdot (1 + s) \\ z_k(3) &= \left[A_{z_b} + v_k(3) + b(3)\right] \cdot (1 + s) \end{aligned}\right\} \quad \text{(C66)}$$

where

s = scale factor error = .0025

$b(2) = b(3)$ = bias = 0.32 ft/sec^2

$v_k(2), v_k(3)$ = zero mean Gaussian noise

$E\{v_k^2(2)\} = E\{v_k^2(3)\} = (0.32 \text{ ft/sec}^2)^2$

Pitch rate.- The pitch rate measurement includes only a noise error.

$$z_k(4) = q + v_k(4) \quad \text{(C67)}$$

where

q = pitch rate = $x_k(4)$

$v_k(4)$ = zero mean Gaussian noise

$E\{v_k^2(4)\} = (.02 \text{ deg/sec})^2$

Air speed.- The air speed measurement includes a multiplicative noise error and a bias.

$$z_k(5) = V_a[1 + v_k(5)] + b(5) \tag{C68}$$

where

$V_a = U_o(1 + u' + u'_W)/\cos(\alpha + \alpha_W)$

u' = normalized inertial velocity along $x = x_k(2)$

u'_W = normalized wind velocity along $x = w_k(1)$

α = angle-of-attack due to inertial velocity along $z = x_k(3)$

α_W = angle-of-attack due to wind velocity along $z = w_k(2)$

$b(5) = 3$ kts

$v_k(5)$ = zero mean Gaussian noise

$E\{v_k^2(5)\} = (0.02)^2$

Altitutde rate.- The altitude rate measurement includes only a noise error.

$$z_k(6) = \dot{h} + v_k(6) \tag{C69}$$

where

$\dot{h} = U_o(1 + u')[\sin(\theta_o + \theta - \alpha_o) - \tan\alpha \cos(\theta_o + \theta - \alpha_o)]$

$v_k(6)$ = zero mean Gaussian noise

$E\{v_k^2(6)\} = (5 \text{ ft/sec})^2$

Angle-of-attack.- The angle-of-attack measurement includes bias and additive noise errors.

$$z_k(7) = \alpha + \alpha_W + v_k(7) + b(7) \tag{C70}$$

where α and α_W were previously defined, and $v_k(7)$ is zero mean Gaussian noise. The bias $b(7)$ and noise error variance were estimated to be $0.25°$ and $(0.4°)^2$, respectively.

The measurement errors are summarized in table C1.

TABLE C1.- MEASUREMENT ERRORS

Measurement	Error type			
	Noise standard deviation	Bias	Scale factor	Alignment
Pitch	0.23°	0.23°	-	-
Acceleration	0.32 $\frac{ft}{sec^2}$	0.32 $\frac{ft}{sec^2}$	0.0025	0.2°
Pitch rate	0.02 $\frac{deg}{sec}$	-	-	-
Air speed	0.02*	3.0 kts	-	-
Altitude rate	5 $\frac{ft}{sec}$	-	-	-
Angle-of-attack	0.4°	0.25°	-	-

*multiplicative

Implementation

Implementation of these equations into the simulation requires evaluation of the integrals in the expressions for Γ_W, R_ξ, and R_η in equations (C55), (C50), and (C60), respectively. The integrals in equations (C55) and (C50) and the inner integrals in equation (C60) were evaluated using a Langley software library subroutine GLEGEN, which performs numerical integration using a Gauss-Legendre formula. The outer integral in equation (C60) was evaluated using the library subroutine SIMP, which performs numerical integration using Simpson's formula. In all cases, the aircraft transition matrix was evaluated using the library subroutine CONEXP, which computes the matrix exponential.

Random sequences.- The random sequences ξ_k and η_k have correlation matrices R_ξ and R_η defined by equations (C50) and (C60), respectively. In general, these matrices are not diagonal, and thus the components $\xi_k(1)$, $\xi_k(2)$, ..., $\xi_k(6)$ of the vector ξ_k are not independent as they were with the vector $\xi(t)$ in the continuous time case. This is also true of the components $\eta_k(1)$, $\eta_k(2)$, ..., $\eta_k(6)$ of η_k.

At time t_k the simulation generates a vector ξ_k of six random numbers with covariance matrix R_ξ using the following technique. Let x be a vector of zero

mean, independent, Gaussian random variables with unity variance. Then the correlation matrix R_x is

$$R_x = E\{xx^T\}$$
$$= I \tag{C71}$$

Let y be the vector of desired zero mean random variables $y_1, y_2, \ldots, y_N$ with the covariance matrix R_y. Now let the desired random vector y be given by

$$y = Gx \tag{C72}$$

where the transformation G is defined to produce the desired covariance of y, that is

$$E\{yy^T\} = E\{Gxx^TG^T\}$$
$$= GE\{xx^T\}G^T \tag{C73}$$
$$= GG^T$$

Therefore

$$GG^T = R_y \tag{C74}$$

If G is assumed to be triangular, one solution (of many) to equation (C74) is given by the following:

$$y_1 = g_{11}x_1$$
$$y_2 = g_{21}x_1 + g_{22}x_2$$
$$\vdots \tag{C75}$$
$$y_N = g_{N1}x_1 + g_{N2}x_2 + \cdots + g_{NN}x_N$$

Then

$$E\{y_1^2\} = R_{11} = g_{11}^2$$

$$E\{y_2 y_1\} = R_{21} = g_{11}g_{21}$$

$$E\{y_2^2\} = R_{22} = g_{21}^2 + g_{22}^2 \qquad \text{(C76)}$$

$$\vdots$$

This system of equations can be solved for the elements g_{ij} to give

$$g_{11} = \sqrt{R_{11}}$$

$$g_{j1} = R_{j1}/g_{11} \qquad 2 \leq j \leq N$$

$$g_{ji} = \left(R_{ji} - \sum_{m=1}^{i-1} g_{jm}g_{im}\right)\Big/ g_{ii} \qquad 1 < i < j \qquad \text{(C77)}$$

$$g_{jj} = \left\{R_{jj} - \sum_{m=1}^{j-1} g_{jm}^2\right\}^{1/2} \qquad 2 \leq j \leq N$$

The same technique is used to generate the vector η_k of random numbers with covariance R_η.

Failures.- Failures in the control elements were simulated as steps or ramps in the state variables according to

$$x_{k+1} = \phi x_k + \psi u_k + \Gamma_w w_k + \eta_k + \alpha_k f_i \delta_{k+1,\theta} \qquad \text{(C78)}$$

where

$f_i = \psi_i$

= i-th column of the control transition matrix.

and α_k is chosen to be a step or ramp.

Because the acceleration measurements $z_k(2)$ and $z_k(3)$ contain terms which include the continuous time control input matrix B as in equations (C64) through (C66), any failure affecting these terms must be accounted for in the simulated measurements. For the four failures simulated, only the elevator and spoiler failures affected the B-matrix and thus introduced failure effects directly into the measurement equation via the expressions for $\dot{u}'$ and $\dot{\alpha}$. For a stuck actuator these effects were simulated by adding terms to equation (C64) as follows:

$$\dot{u}' = \varepsilon_2^T \{Ax_k + Bu_k + Dw_k + B_i[\alpha_k - u_k(i)]\}$$

$$\dot{\alpha} = \varepsilon_3^T \{Ax_k + Bu_k + Dw_k + B_i[\alpha_k - u_k(i)]\} \qquad \text{(C79)}$$

where

B_i = i-th column of B

$u_k(i)$ = i-th component of the control vector u_k

The term $B_i\alpha_k$ accounts for the failure and the term $B_i u_k(i)$ accounts for the loss of that control input.

APPENDIX D

THE KALMAN FILTER

As described in appendices A and B, to perform the FDI computations the GLR technique uses the innovations from a discrete time Kalman Filter, which estimates the system states. As discussed in the Results section of this report, a brief investigation was conducted to evaluate the performance of the GLR algorithm as a function of the number of states in the filter. From the results of this investigation it was decided for this work to have a 10-state Kalman Filter estimate the wind gusts as well as the aircraft states. This appendix discusses the implementation of this filter.

The System Model

The model of the system which the Kalman Filter is designed to estimate must include the dynamics of the aircraft and of the wind. This is accomplished by combining the aircraft dynamics in equation (C54) and the wind gust dynamics in equation (C44) into one state equation as follows:

$$x^F_{k+1} = \phi_F x^F_k + \psi_F u_k + \Gamma_F \zeta_k \tag{D1}$$

where the combined system state vector is defined by

$$x^F_k = \begin{bmatrix} x^F_k(1) \\ x^F_k(2) \\ x^F_k(3) \\ x^F_k(4) \\ x^F_k(5) \\ x^F_k(6) \\ x^F_k(7) \\ x^F_k(8) \\ x^F_k(9) \\ x^F_k(10) \end{bmatrix} = \begin{bmatrix} x_k(1) \\ x_k(2) \\ x_k(3) \\ x_k(4) \\ x_k(5) \\ x_k(6) \\ W_k(1) \\ W_k(2) \\ W_k(3) \\ W_k(4) \end{bmatrix} = \begin{bmatrix} \theta \\ u' \\ \alpha \\ q \\ \delta T \\ \delta S \\ -\alpha_g \\ * \\ * \\ -u'_g \end{bmatrix} \tag{D2}$$

The control vector for the combined system is the same as for the aircraft system and is defined as in equation (C3) by

$$u_k = \begin{bmatrix} u_k(1) \\ u_k(2) \\ u_k(3) \\ u_k(4) \end{bmatrix} = \begin{bmatrix} \delta e \\ \delta th \\ \delta st \\ \delta sp \end{bmatrix} \tag{D3}$$

The plant disturbance vector (winds) is a combination of the white Gaussian noise vector sequence η_k and the gust components of the white Gaussian noise sequence ξ_k defined by equations (C56) and (C46), respectively.

$$\xi_k = \begin{bmatrix} \eta_k(1) \\ \eta_k(2) \\ \eta_k(3) \\ \eta_k(4) \\ \eta_k(5) \\ \eta_k(6) \\ \xi_k(1) \\ \xi_k(2) \\ \xi_k(3) \\ \xi_k(4) \end{bmatrix} \tag{D4}$$

The combined system transition matrix is

$$\phi_F = \left[\begin{array}{c|c} \phi & \Gamma_w^F \\ \hline 0 & \phi_w^F \end{array}\right] \tag{D5}$$

where ϕ is the aircraft system transition matrix defined by equation (C39), ϕ_w^F is the upper left 4 × 4 sub-matrix of the wind system transition matrix defined by

equation (C45), and Γ_w^F is the first four columns of the matrix defined by equation (C55). The combined control transition matrix is defined by

$$\psi_F = \begin{bmatrix} \psi \\ \hline 0 \end{bmatrix} \tag{D6}$$

where ψ is the aircraft control transition matrix defined by equation (C42). The combined disturbance transtion matrix is the identity matrix.

$$\Gamma_F = I \tag{D7}$$

The plant noise covariance is modeled by

$$E(\zeta_j \ \zeta_k^T) = R_\zeta \ \delta_{jk} \tag{D8}$$

$$R_\zeta = \left[\begin{array}{c|c} R_\eta & 0 \\ \hline 0 & R'_\xi \end{array}\right] \tag{D9}$$

where R_η and R'_ξ are the covariances of η_k and ξ'_k, respectively. R_η is defined by equation (C60), and R'_ξ is the upper left 4 x 4 sub-matrix of the matrix defined by equation (C50).

For use in the Kalman Filter design the system measurements, or observations, are modeled as linear combinations of the system state plus additive Gaussian noise.

$$y_{k+1} = Hx^F_{k+1} + v^F_{k+1} \tag{D10}$$

The actual measurements, as described in appendix C, are not linear functions of the state in all cases. A pre-processor, to be described later, is used to convert the measurements z_k into a vector y_k of observations, or pseudo-measurements, which can then be approximated as linear functions of the state.

The Filter

The Kalman Filter is defined by the equations

$$\hat{x}(k+1|k) = \phi_F \hat{x}(k|k) + \psi_F u_k \tag{D11}$$

$$\hat{x}(k|k) = \hat{x}(k|k-1) + K\,\gamma(k) \tag{D12}$$

where K is the Kalman gain. The innovations $\gamma(k)$ are related to the observations by the following:

$$\gamma(k) = y_k - H\hat{x}(k|k-1) \tag{D13}$$

A constant gain filter was used to greatly reduce the computational workload. Constant gain could be used since the aircraft system matrices are constant, or very slowly changing, for a given flight segment. The wind covariance may vary more rapidly, but since it is also not accurately known, a constant value was used. The filter gain K was computed using the subroutine ASYMFIL from the linear control system design software package ORACLS (ref. 22).

The Pre-Processor

As previously noted, the actual measurements z_k are not all linear functions of the state. A pre-processor was used to obtain from the measurements a set of observations y_k which could be approximated by a linear model as in equation (D10). This pre-processor is described in the following paragraphs.

Pitch.- From equation (C62) the output of the pitch attitude gyro is

$$z_k(1) = \theta + v_k(1) + b(1)$$

In this case it suffices to let

$$y_k(1) = z_k(1) \tag{D14}$$

and then $y_k(1)$ can be modeled as

$$y_k(1) = \theta + v_k^F(1)$$

$$= x_k^F(1) + v_k^F(1) \tag{D15}$$

Accelerations.- The outputs of the body mounted accelerometers are given by equations (C63) through (C66). The first step in pre-processing these measurements is to convert them to stability coordinates according to

$$A^F_{xs} = z_k(2) \cos \alpha^F_o + z_k(3) \sin \alpha^F_o$$

$$A^F_{zs} = -z_k(2) \sin \alpha^F_o + z_k(3) \cos \alpha^F_o \qquad \text{(D16)}$$

where α^F_o = trim angle-of-attack in the combined system model

Comparison of the stability axis accelerations in equations (D16) with those in (C65) shows that

$$A^F_{xs} = A_{xs} + e_x$$

$$A^F_{zs} = A_{zs} + e_z \qquad \text{(D17)}$$

where e_x is an error term due to accelerometer noise $v_k(2)$, bias error $b(2)$, scale factor error s, accelerometer alignment error a, and error $(\alpha_o - \alpha^F_o)$ in the trim angle-of-attack. From equations (C63) and (C64)

$$A^F_{xs} = U_o \varepsilon_2^T (Ax_k + Bu_k + Dw_k) + qU_o \tan \alpha + g \sin (\theta_o + \theta - \alpha_o)$$

$$A^F_{zs} = U_o \tan \alpha \, \varepsilon_2^T (Ax_k + Bu_k + Dw_k) - qU_o - g \cos(\theta_o + \theta - \alpha_o) \qquad \text{(D18)}$$

$$+ [(1 + u')U_o/\cos^2 \alpha] \cdot \varepsilon_3^T (Ax_k + Bu_k + Dw_k)$$

Define the observations $y_k(2)$ and $y_k(3)$ as follows:

$$y_k(2) = \frac{1}{U^F_o} [A^F_{xs} - g \sin (\theta^F_o - \alpha^F_o)] - \varepsilon_3^T B_F u_k$$

$$y_k(3) = \frac{1}{U^F_o} [A^F_{zs} + g \cos (\theta^F_o - \alpha^F_o)] - \varepsilon_3^T B_F u_k \qquad \text{(D19)}$$

The pre-processor then calculates the observations $y_k(2)$ and $y_k(3)$ from the measurements $z_k(2)$ and $z_k(3)$ using equations (D16) and (D19). From equations (D18) and (D19) these observations can be approximated as linear functions of the states as follows:

$$y_k(2) \approx q \tan \alpha + \varepsilon_2^T [A_F x_k + D_F w_k]$$

$$+ \left(g/U_o^F\right) \cos\left(\theta_o^F - \alpha_o^F\right) \sin \theta + v_k^F(2)$$

$$\approx \sum_{j=1}^{6} A_F(2,j)\, x_k^F(j) + \sum_{j=1}^{6} D_{co}(2,j)\, x_k^F(j+6)$$

$$+ \left(g/U_o^F\right) \cos\left(\theta_o^F - \alpha_o^F\right)\, x_k^F(1) + v_k^F(2) \qquad \text{(D20)}$$

$$y_k(3) \approx -q + \tan \alpha \cdot \varepsilon_2^T [A_F x_k + D_F w_k]$$

$$+ [(1 + u')/\cos^2 \alpha] \cdot \varepsilon_3^T [A_F x_k + D_F w_k] + v_k^F(3)$$

$$+ (g/U_o) \sin\left(\theta_o^F - \alpha_o^F\right) \sin \theta$$

$$\approx -x_k^F(4) + \left(g/U_o^F\right) \sin\left(\theta_o^R - \alpha_o^F\right) x_k^F(1)$$

$$+ \sum_{j=1}^{6} A_F(3,j)\, x_k^F(j) + \sum_{j=1}^{6} D_{co}(3,j)\, x_k^F(j+6) + v_k^F(3) \qquad \text{(D21)}$$

where

$$D_{co} = D^F C_{wo}^F \qquad \text{(D22)}$$

and

$$C_{co}^{F} = C_{w}^{F}\Big|_{\theta=0}$$

$$= \begin{bmatrix} -\sin\alpha_o^F & 0 & 0 & -\cos\alpha_o^F & -\cos(\theta_o^F - \alpha_o^F) & \sin(\theta_o^F - \alpha_o^F) \\ -\cos\alpha_o^F & 0 & 0 & \sin\alpha_o^F & -\sin(\theta_o^F - \alpha_o^F) & -\cos(\theta_o^F - \alpha_o^F) \\ -\frac{\pi V_a^F}{4b} & 0 & \frac{\pi V_a^F}{4b} & 0 & 0 & 0 \end{bmatrix} \quad \text{(D23)}$$

Pitch rate.- From equation (C64) the output of the pitch rate gyro is

$$z_k(4) = q + v_k(4)$$

It is sufficient to let

$$y_k(4) = z_k(4) \quad \text{(D24)}$$

which case $y_k(4)$ can be modeled as

$$y_k(4) = x_k^F(4) + v_k^F(4) \quad \text{(D25)}$$

Air speed.- From equation (C68) the air speed measurement is

$$z_k(5) = V_a[1\ v_k(5)] + b(5)$$

$$= U_o\left[(1 + u' + u_w')/\cos(\alpha + \alpha_w)\right] \cdot [1 + v_k(5)] + b(5)$$

Define the air speed observation as

$$y_k(5) = \left[z_k(5)/U_o^F\right] - 1 \quad \text{(D26)}$$

The observation can be approximated as a linear combination of the states as follows:

$$y_k(5) = \left[\frac{1 + u' + u'_w}{\cos(\alpha + \alpha_x)}\right][1 + v_k(5)] + \frac{b(5)}{U_o} - 1$$

$$\approx u' + u'_w + v^F_k(5)$$

$$\approx x^F_k(2) + \sum_{j=1}^{6} C_{wo}(1,j)\, x^F_k(j+6) + v^F_k(5) \qquad \text{(D27)}$$

Altitude rate.- From equation (C69) the altitude rate measurment is

$$z_k(6) = \dot{h} + v_k(6)$$

$$= U_o(1 + u')\,[\sin(\theta_o + \theta - \alpha_o) - \tan\alpha \cos(\theta_o + \theta - \alpha_o)] + v_k(6)$$

Define the observation

$$y_k(6) = [z_k(6)/U^F_o] - (\theta^F_o - \alpha^F_o) \qquad \text{(D28)}$$

which can be approximately modeled as

$$y_k(6) \approx (1 + u')\big[\sin(\theta^F_o - \alpha^F_o)\cos\theta + \cos(\theta^F_o - \alpha^F_o)\sin\theta$$

$$- \tan\alpha \cos(\theta^F_o - \alpha^F_o)\cos\theta + \tan\alpha \sin(\theta^F_o - \alpha^F_o)\sin\theta\big]$$

$$+ v_k(6)/U^F_o - (\theta^F_o - \alpha^F_o)$$

$$\approx u' \sin(\theta^F_o - \alpha^F_o) + \cos(\theta^F_o - \alpha^F_o)\,\theta - \alpha + v^F_k(6)$$

$$\approx (\theta^F_o - \alpha^F_o)\, x^F_k(2) + x^F_k(1) - x^F_k(3) + v^F_k(6) \qquad \text{(D29)}$$

Angle-of-attack.- From equation (C70) the output of the angle-of-attack sensor is

$$z_k(7) = \alpha + \alpha_w + v_k(7) + b(7)$$

Define the observation

$$y_k(7) = z_k(7) \tag{D30}$$

which can be modeled by

$$y_k(7) = \alpha + \alpha_w + v_k^F(7)$$

$$\approx x_k^F(3) + \sum_{j=1}^{6} C_{wo}(2,j)\, x_k^F(j+6) + v_k^F(7) \tag{D31}$$

The pre-processor computes the obsrvations y_k from the measurements z_k according to equations (D14), (D16), (D19), (D24), (D26), (D28), and (D30). These observations are the inputs to the Kalman Filter. For use in the filter algorithms the observations can now be expressed as in equation (D10) with the observation matrix defined by equation (D32).

$$
H_F = \begin{bmatrix}
1 & 0 & 0 & 0 & 0 & 0 & 0 & 0 & 0 & 0 \\
A_F(2,1) + \frac{9}{U_o^F}\cos\left(\theta_o^F - \alpha_o^F\right) & A_F(2,2) & A_F(2,3) & A_F(2,4) & A_F(2,5) & A_F(2,6) & D_{CO}(2,1) & D_{CO}(2,2) & D_{CO}(2,3) & D_{CO}(2,4) \\
A_F(3,1) + \frac{9}{U_o^F}\sin\left(\theta_o^F - \alpha_o^F\right) & A_F(3,2) & A_F(3,3) & \begin{pmatrix} A_F(3,4) \\ -1 \end{pmatrix} & A_F(3,5) & A_F(3,6) & D_{CO}(3,1) & D_{CO}(3,2) & D_{CO}(3,3) & D_{CO}(3,4) \\
0 & 0 & 0 & 1 & 0 & 0 & 0 & 0 & 0 & 0 \\
0 & 1 & 0 & 0 & 0 & 0 & C_{WO}(1,1) & C_{WO}(1,2) & C_{WO}(1,3) & C_{WO}(1,4) \\
1 & \left(\theta_o^F - \alpha_o^F\right) & -1 & 0 & 0 & 0 & 0 & 0 & 0 & 0 \\
0 & 0 & 1 & 0 & 0 & 0 & C_{WO}(2,1) & C_{WO}(2,2) & C_{WO}(2,3) & C_{WO}(2,4)
\end{bmatrix} \qquad \text{(D32}
$$

REFERENCES

1. Willsky, Alan S.: A Survey of Design Methods for Failure Detection in Dynamic Systems. Automatica, vol. 12, 1976, pp. 601-611.

2. Chow, Edward Y.: Failure Detection System Design Methodology. LIDS-TH-1055, Lab. for Info. and Decision Sciences, MIT, Oct. 1980.

3. Chow, Edward Y.; and Willsky, Alan S.: Issues in the Development of a General Design Algorithm for Reliable Failure Detection. 19th IEEE Conf. on Decision and Cont., 1980, pp. 1006-1012.

4. Motyka, Paul; Landey, M.; and McKern, R.: Failure Detection and Isolation Analysis of a Redundant Strapdown Inertial Measurement Unit. (R-1414, C. S. Draper Lab.; NAS1-15933.) NASA CR-165658, Feb. 1981.

5. Deyst, J.; et. al.: Development and Testing of Advanced Redundancy Management Methods for the F-8 DFBW Aircraft. 1977 IEEE Conf. on Decision and Cont., pp. 309-315.

6. Caglayan, Alper K.; and Lancraft, Roy E.: An Aircraft Sensor Fault Tolerant System. (Rept. No. 4858, Bolt Beranek and Newman; NAS1-16579.) NASA CR-165876, April 1982.

7. Friedland, Bernard: Maximum Likelihood Failure Detection of Aircraft Flight Control Sensors. AIAA 82-4252, J. of Guid., Cont.,and Dynamics, vol. 5, no. 5, 1982, pp. 498-503.

8. Beard, Richard V.: Failure Accommodation in Linear Syatems Through Self-Reorganization. Ph.D. Thesis, MIT, 1971.

9. Jones, Harold Lee: Failure Detection in Linear Systems. Ph.D. Thesis, MIT, 1973.

10. Meserole, Jere S.: Detection Filters for Fault-Tolerant Control of Turbofan Engines. Ph.D. Thesis, MIT, 1981.

11. Willsky, Alan S.; and Jones, Harold L.: A Generalized Likelihood Ratio Approach to State Estimation in Linear Systems Subject to Abrupt Changes. 1974 IEEE Conf. on Decision and Cont., Paper No. FP4.3, pp. 846-853.

12. Chow, Edward; Dunn, Keh-Ping; and Willsky, Alan S.: A Dual-Model Generalized Likelihood Ratio Approach to Self-Reorganizing Digital Flight Control System Design. Research Status Rept. No. 1, Electronic Sys. Lab., MIT, April 14, 1975.

13. Bueno, Ramon; et. al.: A Dual-Mode Generalized Likelihood Ratio Approach to Self-Reorganizing Digital Flight Control System Design. (Research Status Rept. No. 2, ESL-IR-642, Electronic Sys. Lab., MIT; NASA Grant NSG-1112.) NASA CR-146386, 1975.

14. Bueno, Ramon A.: Performance and Sensitivity Analysis of the Generalized Likelihood Ratio Method for Failure Detection. (M.S. Thesis, ESL-R-706, Electronic Sys. Lab., MIT; NASA Grant NSG-1112.) NASA CR-149272, 1977.

15. Anon.: A Dual-Mode Generalized Likelihood Approach to Self-Reorganizing Digital Flight Control System Design. (ESL-FR-707, Electronic Sys. Lab., MIT; NASA Grant NSG-1112.) NASA CR-149317, 1977.

16. Liu, Jack S.; and Jones, Harold L.: Linear Manifold Constrained GLR. IEEE Trans. Auto. Cont., vol. AC-22, no. 6, Dec. 1977, pp. 988-989.

17. Chang, C. B.; and Dunn, K. P.: On GLR Detection and Estimation of Unexpected Inputs in Linear Discrete Systems. IEEE Trans. Auto. Cont., vol. AC-24, no. 3, June 1979, pp. 499-501.

18. Tylee, J. Louis: Bias Identification in PWR Pressurizer Instrumentation Using the Generalized Likelihood Ratio Technique. Paper FA-4B, 1981 Joint Auto. Controls Conf.

19. Halyo, Nesim: Development of an Optimal Automatic Control Law and Filter Algorithm for Steep Glideslope Capture and Glideslope Tracking. NASA CR-2720, 1976.

20. Chalk, C. R.; et. al.: Background Information and User Guide for MIL-F-8785B/ASG/ - Military Specification - Flying Qualities of Piloted Airplanes. Tec. Rept. AFFFDL-TR-69-72, Cornell Aeronautical Lab., August 1969.

21. Ogata, Katsuhiko: State Space Analysis of Control Systems. Prentice Hall, Inc., 1967.

22. Armstrong, Ernest S.: ORACLS: A Design System for Linear Multivariable Control. Marcel Dekker, Inc., 1980.

TABLE III.a.- GLR VALUES FOR 30-SAMPLE WINDOW

Failure		Turbulence			
Type	Magnitude	None	Medium	Heavy	Thunder-storm
Elevator	10°		3584	4256	5332 4080*
	3°	162	144 130	119 131	
	1°	64	54		
Throttle	40°		2862	1656	7869 5953*
	12°	431	345 450	305 688	
	4°	128	101		
Stabilizer	-6°	940	722 1128	762 1894	24010 20310*
	3°	170	172	118	
	-1°	86	70		
Spoiler	8°	825	629	1176	38000 32870*
	3°	178	152 222	443 417	
	1°	77	69		
None	0	57		425	16630

*Used 10 ft/sec steady state wind in the x-direction. Other thunderstorm runs used 39 ft/sec.

TABLE III.b.- GLR VALUES FOR 20-SAMPLE WINDOW

Failure		Turbulence			
Type	Magnitude	None	Medium	Heavy	Thunder-storm
Elevator	10°		3106	4435	6071 4889*
	3°	104	109 106	104 112	
	1°	46	40		
Throttle	40°		2035	1330	11580 9435*
	12°	297	227 312	255 488	
	4°	91	79		
Stabilizer	-6°	757	526 908	686 1540	26080 22840*
	3°	121	140	122	
	-1°	64	56		
Spoiler	8°	573	470	1367	41900 37310*
	3°	129	118 155	505 293	
	1°	58	52		
None	0	42		321	20380

*Used 10 ft/sec steady state wind in the x-direction. Other thunderstorm runs used 39 ft/sec.

TABLE III.c.- GLR VALUES FOR 10-SAMPLE WINDOW

Failure		Turbulence			
Type	Magnitude	None	Medium	Heavy	Thunder-storm
Elevator	10°		1971	3717	10180 9334*
	3°	62	76 70	142 80	
	1°	27	33		
Throttle	40°		1100	784	10870* 9241*
	12°	165	135 168	154 263	
	4°	52	49		
Stabilizer	-6°	456	284 522	388 884	19320 17030*
	3°	67	105	155	
	-1°	42	38		
Spoiler	8°	302	269	804	30900 27670*
	3°	77	74 85	360 169	
	1°	37	35		
None	0	32		230	17030

*Used 10 ft/sec steady state wind in the x-direction. Other thunderstorm runs used 39 ft/sec.

TABLE IV.- FULL GLR FAILURE DETECTION PERFORMANCE WITH THRESHOLDS SET AT NO TURBULENCE LEVEL

Failure		Turbulence			
Type	Magnitude	None	Medium	Heavy	Thunder-storm
Elevator	10°		Y/Y/Y	Y/Y/Y	Y/Y/Y Y/Y/Y
	3°	Y/Y/Y	Y/Y/Y Y/Y/Y	Y/Y/Y Y/Y/Y	
	1°	Y/Y/n	n/n/Y		
Throttle	40°		Y/Y/Y	Y/Y/Y	Y/Y/Y Y/Y/Y
	12°	Y/Y/Y	Y/Y/Y Y/Y/Y	Y/Y/Y Y/Y/Y	
	4°	Y/Y/Y	Y/Y/Y		
Stabilizer	-6°	Y/Y/Y	Y/Y/Y Y/Y/Y	Y/Y/Y Y/Y/Y	Y/Y/Y Y/Y/Y
	3°	Y/Y/Y	Y/Y/Y	Y/Y/Y	
	-1°	Y/Y/Y	Y/Y/Y		
Spoiler	8°	Y/Y/Y	Y/Y/Y	Y/Y/Y	Y/Y/Y Y/Y/Y
	3°	Y/Y/Y	Y/Y/Y Y/Y/Y	Y/Y/Y Y/Y/Y	
	1°	Y/Y/Y	Y/Y/Y		

Y/Y/Y indicates detection using the 30-, 20-, and 10-sample windows.
n indicates failure not detected.

TABLE V.- FULL GLR FAILURE DETECTION PERFORMANCE WITH THRESHOLDS SET AT HEAVY TURBULENCE LEVEL

Failure		Turbulence			
Type	Magnitude	None	Medium	Heavy	Thunder-storm
Elevator	10°		Y/Y/Y	Y/Y/Y	Y/Y/Y Y/Y/Y
	3°	n/n/n	n/n/n n/n/n	n/n/n n/n/n	
	1°	n/n/n	n/n/n		
Throttle	40°		Y/Y/Y	Y/Y/Y	Y/Y/Y Y/Y/Y
	12°	Y/n/n	n/n/n Y/n/n	n/n/n Y/Y/Y	
	4°	n/n/n	n/n/n		
Stabilizer	-6°	Y/Y/Y	Y/Y/Y Y/Y/Y	Y/Y/Y Y/Y/Y	Y/Y/Y Y/Y/Y
	3°	n/n/n	n/n/n	n/n/n	
	-1°	n/n/n	n/n/n		
Spoiler	8°	Y/Y/Y	Y/Y/Y	Y/Y/Y	Y/Y/Y Y/Y/Y
	3°	n/n/n	n/n/n n/n/n	Y/Y/Y n/n/n	
	1°	n/n/n	n/n/n		

Y/Y/Y indicates detection using the 30-, 20-, and 10-sample windows.
n indicates failure not detected.

TABLE VI.- GLR VALUES FOR MISMATCHED FILTER MODEL

Failure		Turbulence			
Type	Magnitude	None	Medium	Heavy	Thunder-storm
Elevator	10°			12320 12830 11880	
	3°				
	1°				
Throttle	40°			13180 9951 5842	
	12°				
	4°				
Stabilizer	-6°			11110 8127 4716	
	3°				
	-1°				
Spoiler	8°			12800 9826 5717	
	3°				
	1°				
None	0			10860 7847 4593	

30-sample window
20-sample window
10-sample window

TABLE VII.- CONSTRAINED GLR FAILURE DETECTION PERFORMANCE WITH THRESHOLDS SET AT HEAVY TURBULENCE LEVEL

Failure		Turbulence			
Type	Magnitude	None	Medium	Heavy	Thunder-storm
Elevator	10°		Y/Y/Y	Y/Y/Y	Y/Y/Y
	3°	Y/Y/Y	n/Y/Y n/Y/Y	n/Y/Y n/Y/Y	
	1°	n/n/n	n/n/n		
Throttle	40°		Y/Y/Y	Y/Y/Y	Y/Y/Y
	12°	n/n/n	n/n/n Y/n/n	n/n/n Y/Y/Y	
	4°	n/n/n	n/n/n		
Stabilizer	-6°		Y/Y/Y	Y/Y/Y	Y/Y/Y
	3°	Y/Y/Y	Y/Y/Y Y/Y/Y	n/n/n Y/Y/Y	
	-1°	n/n/n	n/n/n		
Spoiler	8°		Y/Y/Y	Y/Y/Y	Y/Y/Y
	3°	Y/n/n	Y/n/n Y/n/n	Y/Y/Y Y/n/n	
	1°	n/n/n	n/n/n		

Y/Y/Y indicates detection using the 30-, 20-, and 10-sample windows.
n indicates failure not detected.

TABLE VIII.- CONSTRAINED GLR FAILURE IDENTIFICATION PERFORMANCE: FAILURE VECTOR CORRECTLY IDENTIFIED

Failure		Turbulence			
Type	Magnitude	None	Medium	Heavy	Thunder-storm
Elevator	10°		Y/Y/Y	Y/Y/Y	Y/Y/n
	3°	Y/Y/Y	*/Y/Y */Y/Y	*/Y/Y */Y/Y	
	1°	*/*/*	*/*/*		
Throttle	40°		Y/Y/Y	Y/Y/Y	Y/Y/Y
	12°	*/*/*	*/*/* Y/*/*	*/*/* Y/Y/Y	
	4°	*/*/*	*/*/*		
Stabilizer	-6°		Y/Y/n	Y/Y/n	n/n/n
	3°	Y/Y/n	Y/Y/n Y/Y/n	*/*/* Y/Y/n	
	-1°	*/*/*	*/*/*		
Spoiler	8°		Y/n/n	Y/Y/n	n/n/n
	3°	Y/*/*	Y/*/* Y/*/*	n/Y/n Y/*/*	
	1°	*/*/*	*/*/*		

Y/Y/Y indicates correct identification using the 30-, 20-, and 10-sample windows.
n indicates incorrect identification.
* indicates failure not detected.

TABLE IX.- CONSTRAINED GLR FAILURE IDENTIFICATION PERFORMANCE: PERCENT ERROR IN FAILURE MAGNITUDE ESTIMATE

Failure		Turbulence			
Type	Magnitude	None	Medium	Heavy	Thunder-storm
Elevator	10°		-1.41# -2.58 -0.99	-2.21 -2.30 -0.36	-3.40 2.90 *
	3°	-6.93 -9.13 -4.20	* * -9.80 -7.47 -3.77 6.60	* * -6.00 -4.43 -1.13 14.8	
	1°	* * *	* * *		
Throttle	40°		44.8 92.0 217.0	8.38 54.5 165.0	-288.0 -485.0 -990.0
	12°	* * *	* 88.8 * * * *	* 135.0 * 214.0 * 407.0	
	4°	* * *	* * *		

#For each case the percent errors are listed in order of decreasing data window size; that is, the error for the 30-sample window islisted first, followed by the errors for the 20- and 10-sample windows.

*Indicates failure not detected.

**Indicates failure not correctly identified.

TABLE IX.- Concluded

Failure		Turbulence			
Type	Magnitude	None	Medium	Heavy	Thunder-storm
Stabilizer	-6°		-37.7# -68.3 **	-50.2 -87.2 **	** ** **
	3°	4.80 35.4 **	-3.53 0.97 26.3 36.0 ** **	* 8.10 * 49.0 * **	
	-1°	* * *	* * *		
Spoiler	8°		-0.74 ** **	-2.14 2.23 **	** ** **
	3°	22.4 * *	20.1 27.5 * * * *	** 17.6 47.2 * ** *	
	1°	* * *	* * *		

#For each case the percent errors are listed in order of decreasing data window size; that is, the error for the 30-sample window is listed first, followed by the errors for the 20- and 10-sample windows.

*Indicates failure not detected.

**Indicates failure not correctly identified.

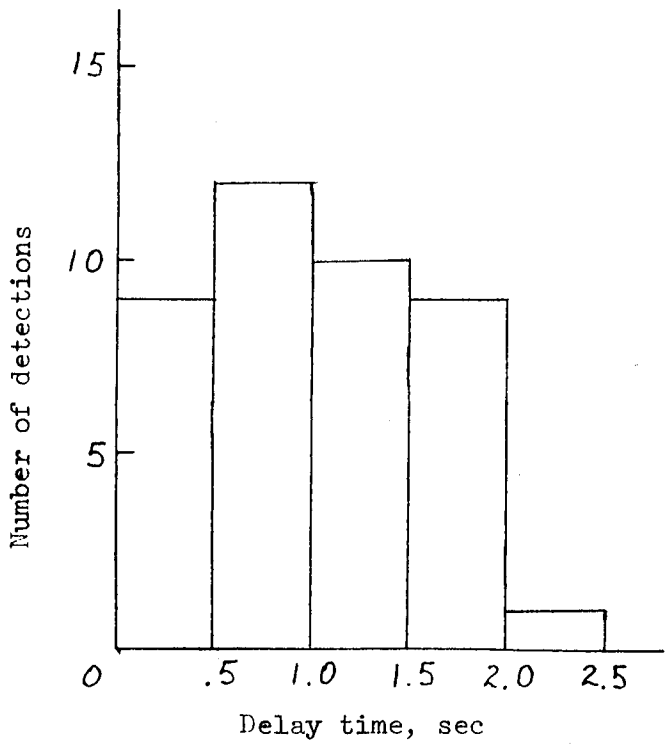

Figure 1.- Histogram of delay time between failure occurrence and failure detection for full GLR.

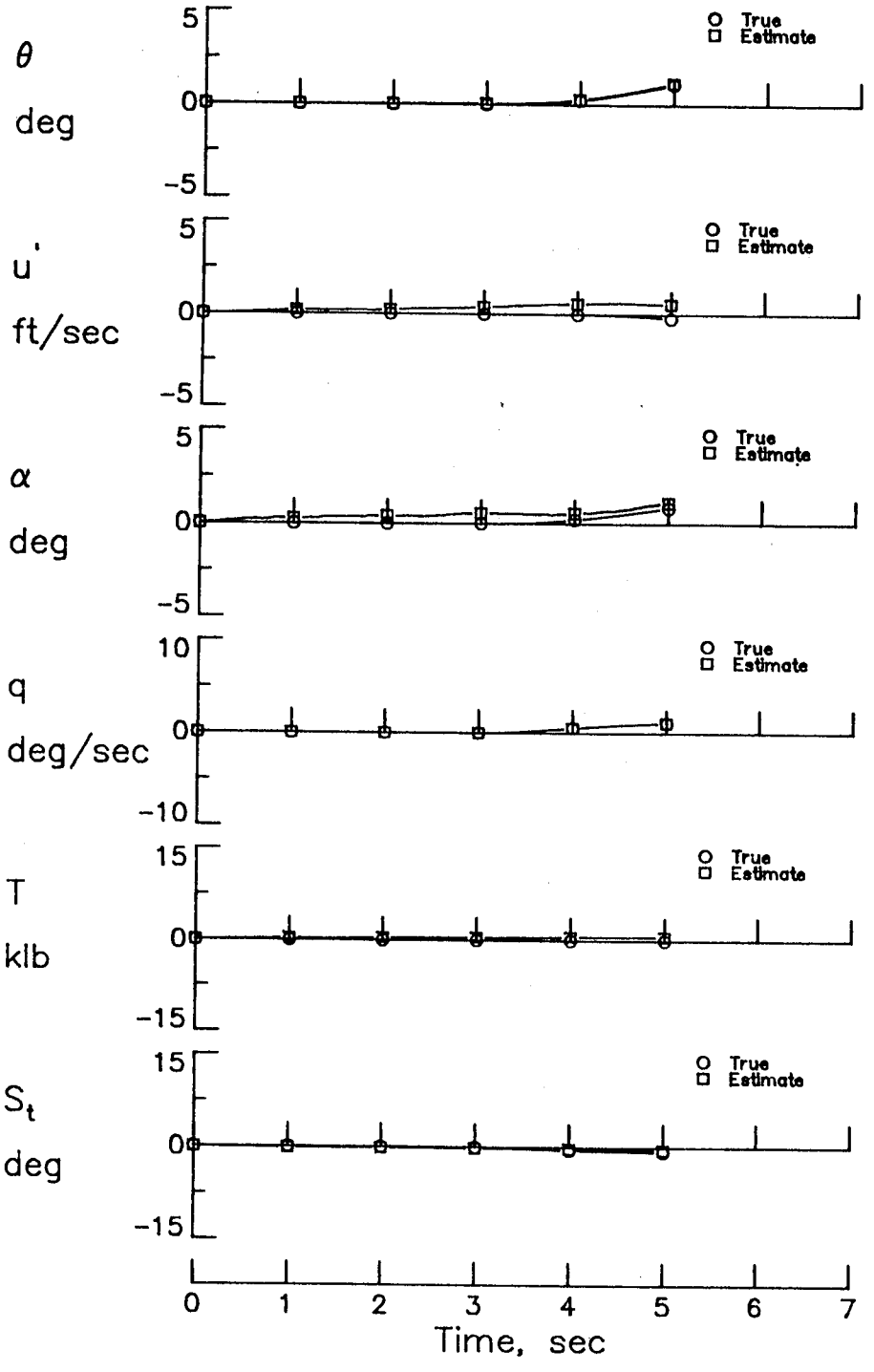

(a) Aircraft states.

Figure 2.- Full GLR results with no turbulence and -1° stabilizer failure at 3 seconds.

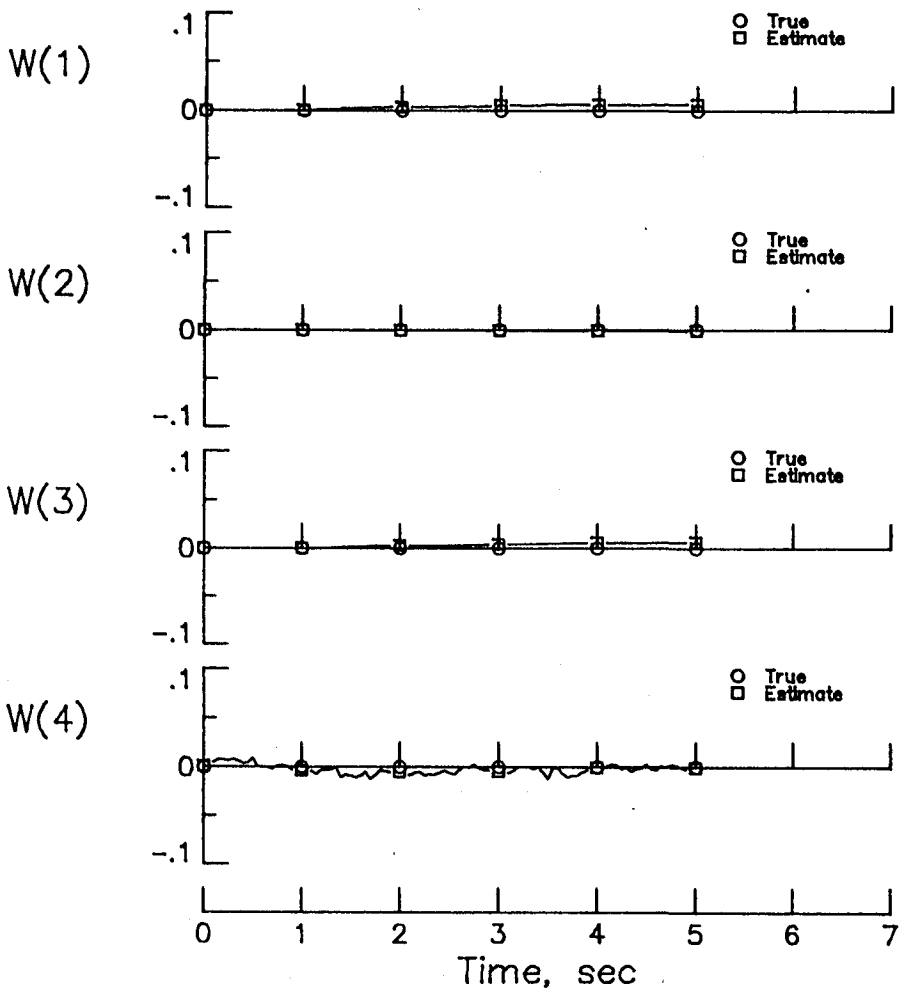

(b) Wind states.

Figure 2.- Continued.

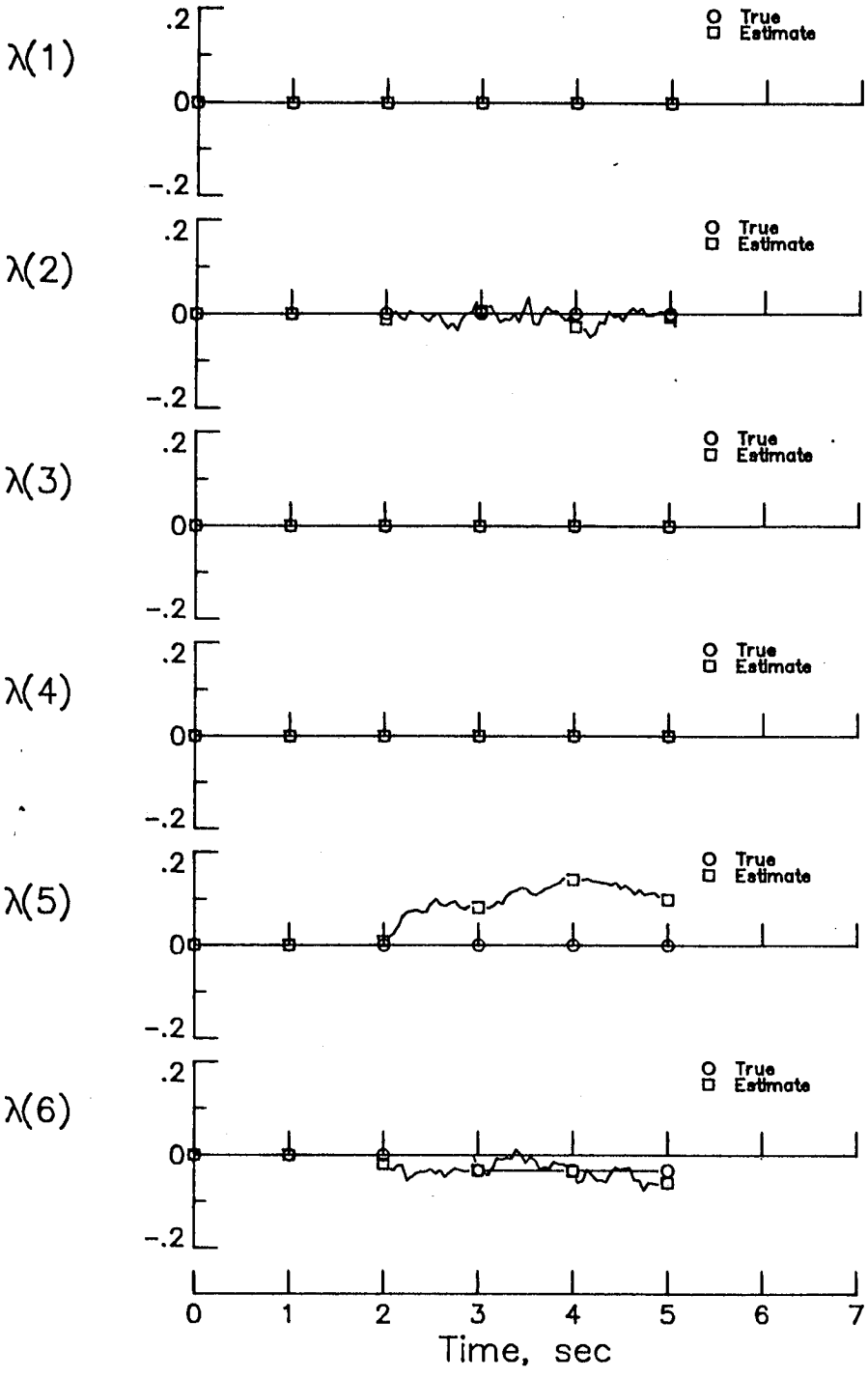

(c) Failure vector.

Figure 2.- Continued.

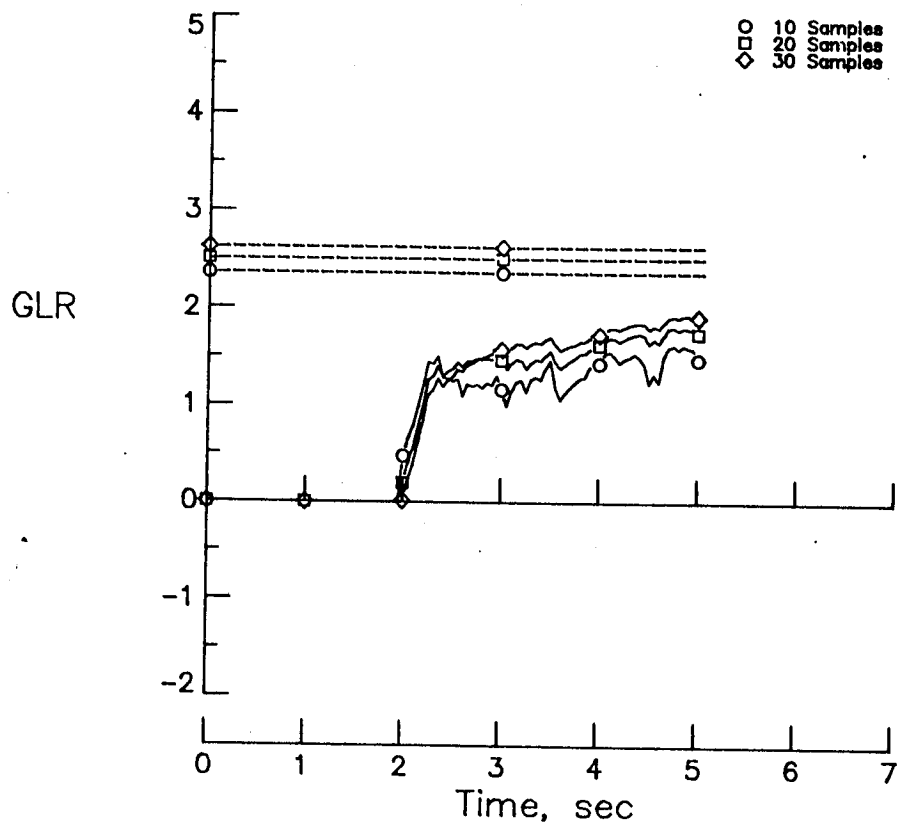

(d) Generalized likelihood ratios.

Figure 2.- Concluded.

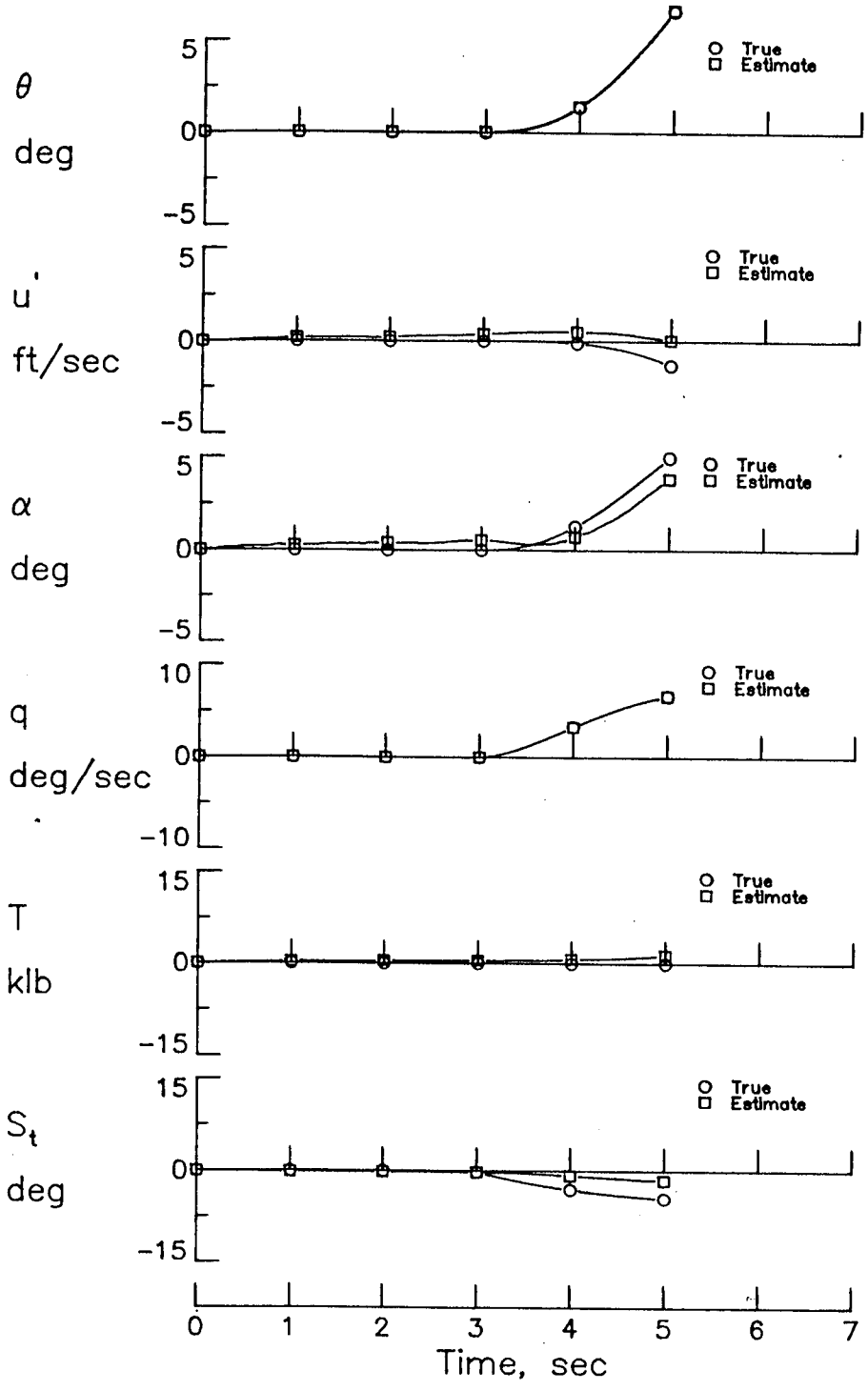

(a) Aircraft states

Figure 3.- Full GLR results with no turbulence and -6° stabilizer failure at 3 seconds.

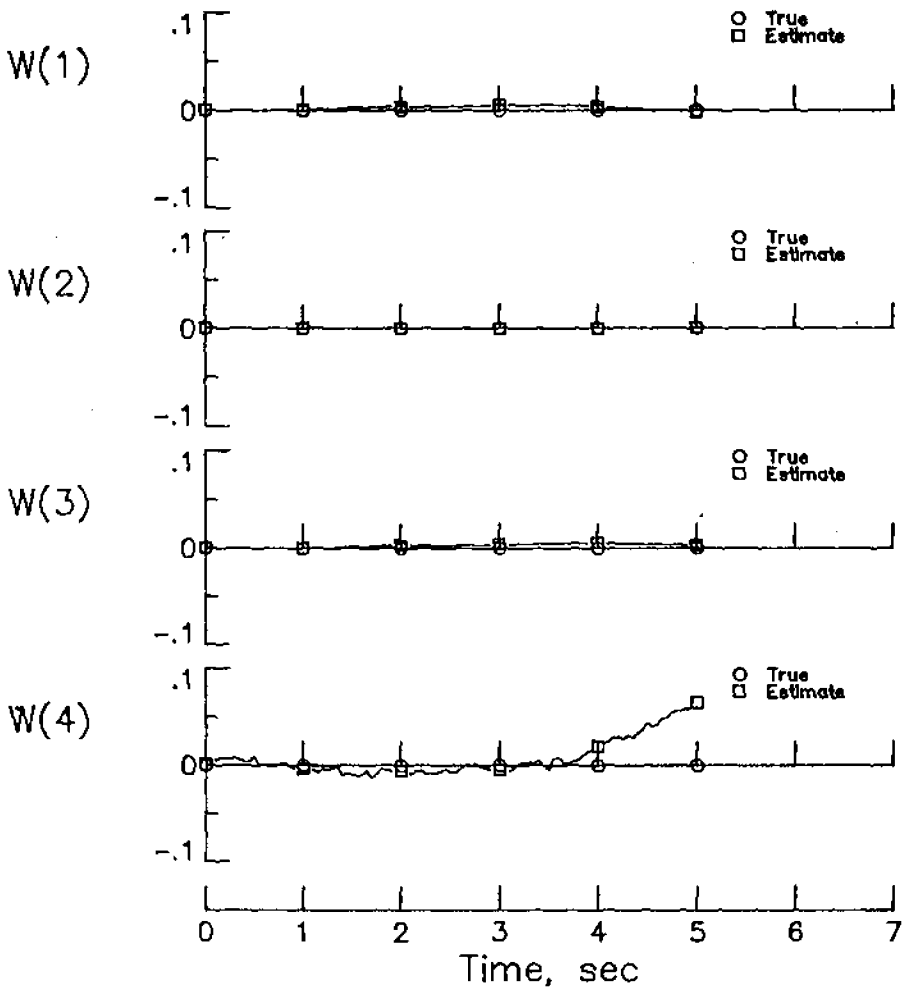

(b) Wind states.

Figure 3.- Continued.

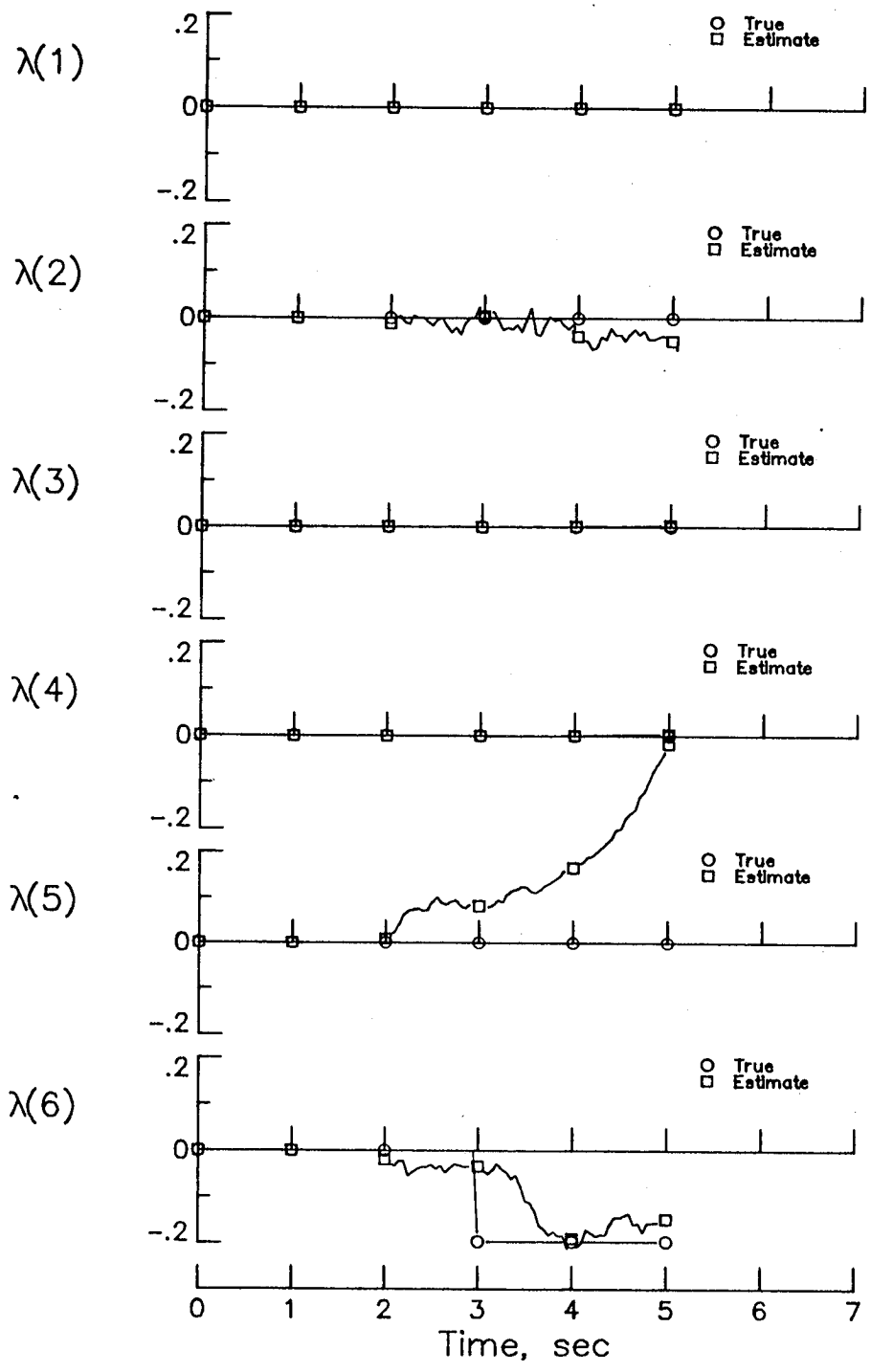

(c) Failure vector.

Figure 3.- Continued.

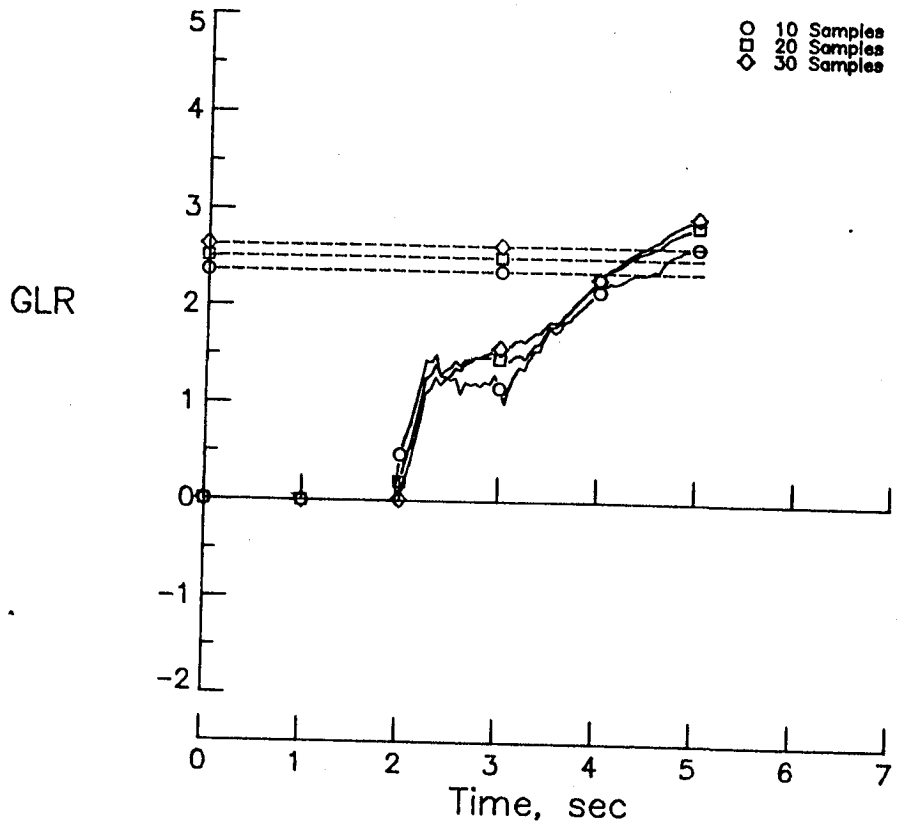

(d) Generalized likelihood ratios.

Figure 3.- Concluded.

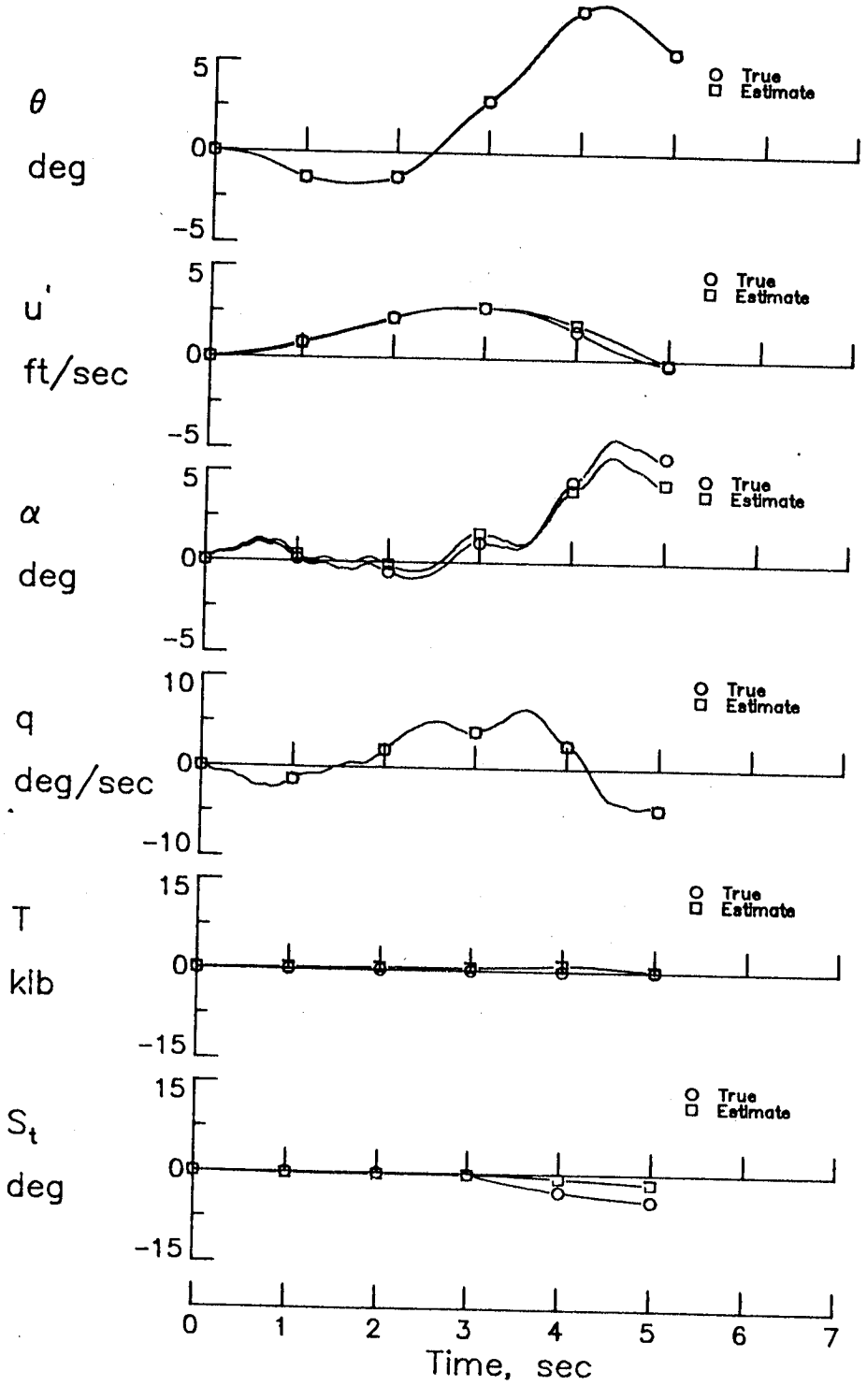

(a) Aircraft states.

Figure 4.- Full GLR results with turbulence ($\sigma_u = \sigma_w = 7.0$ ft/sec) and -6° stabilizer failure at 3 seconds.

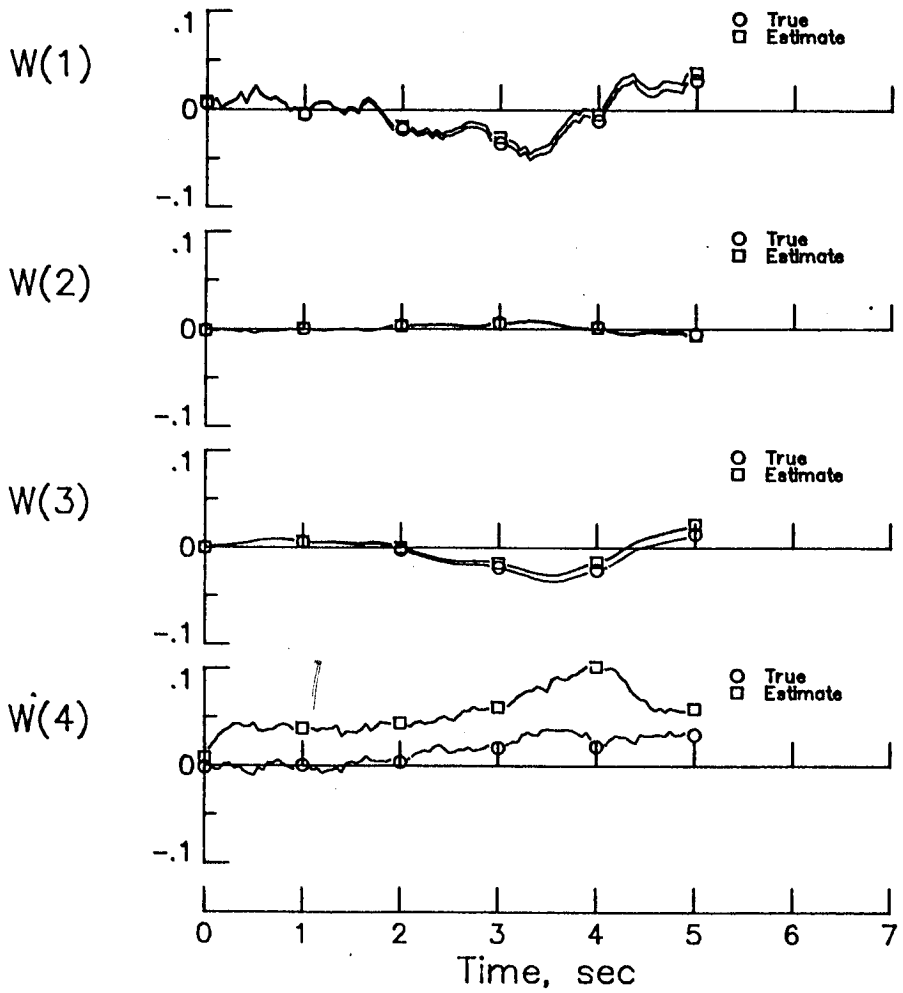

(b) Wind states.

Figure 4.- Continued.

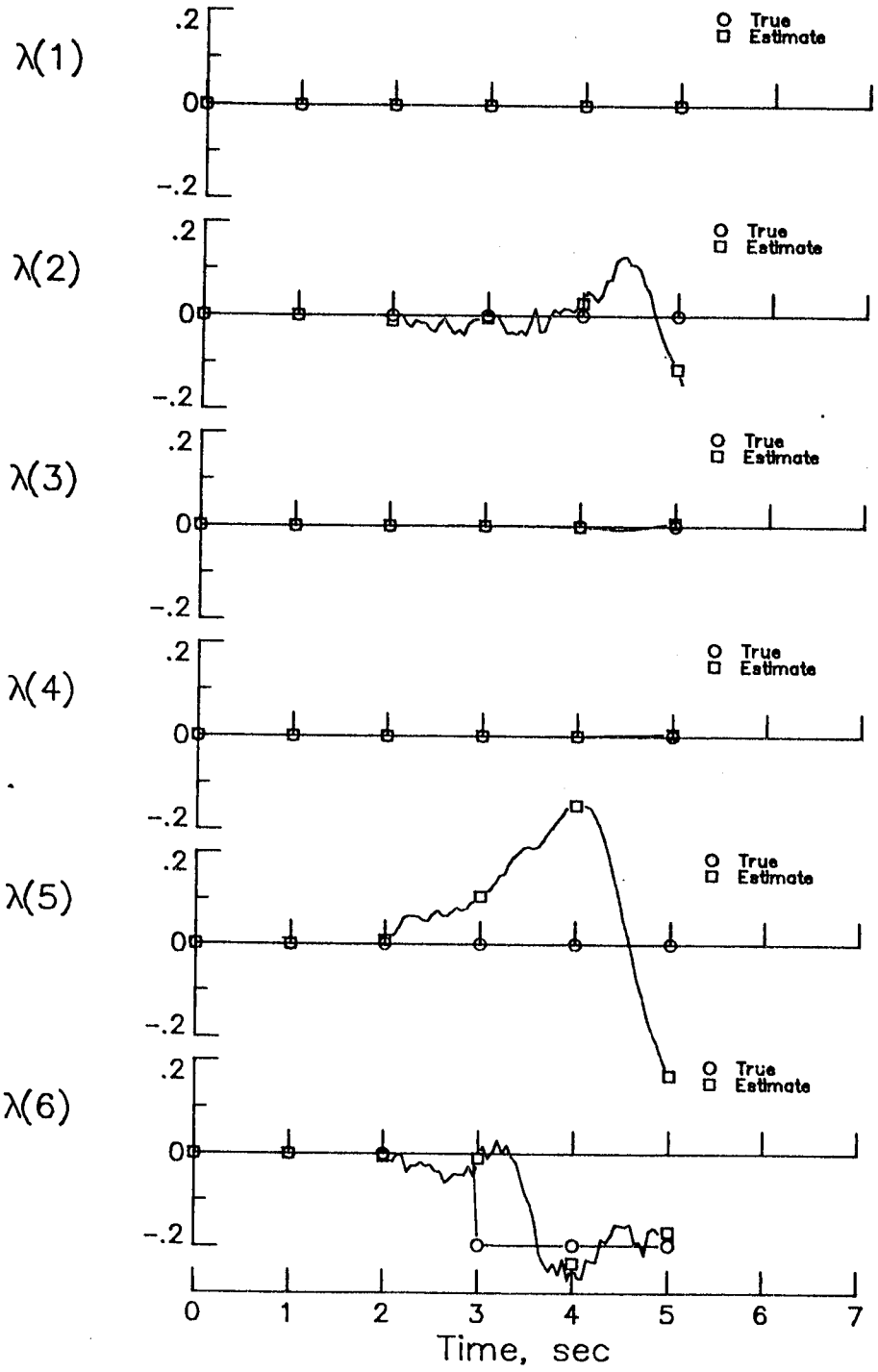

(c) Failure vector.

Figure 4.- Continued.

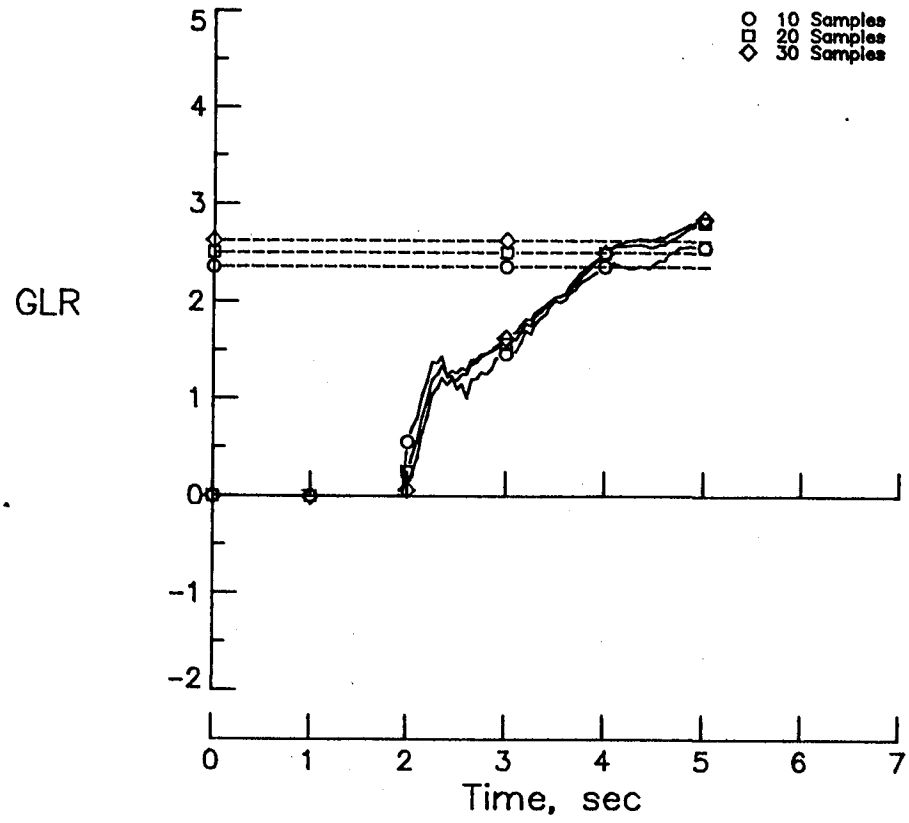

(d) Generalized likelihood ratios.

Figure 4.- Concluded.

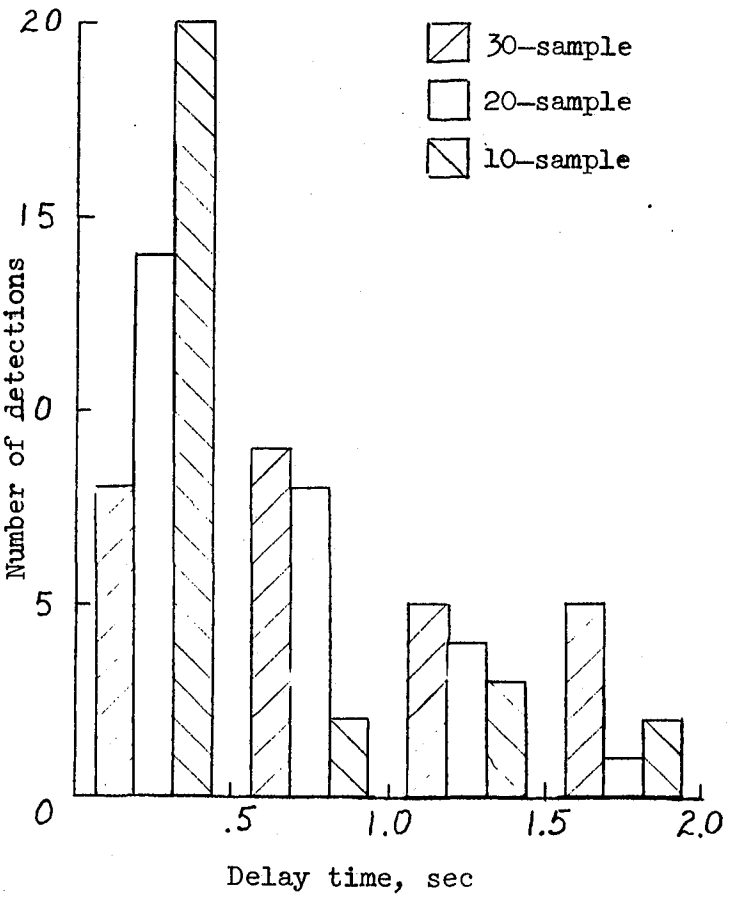

Figure 5.- Histogram of delay time between failure occurrence and failure detection for constrained GLR.

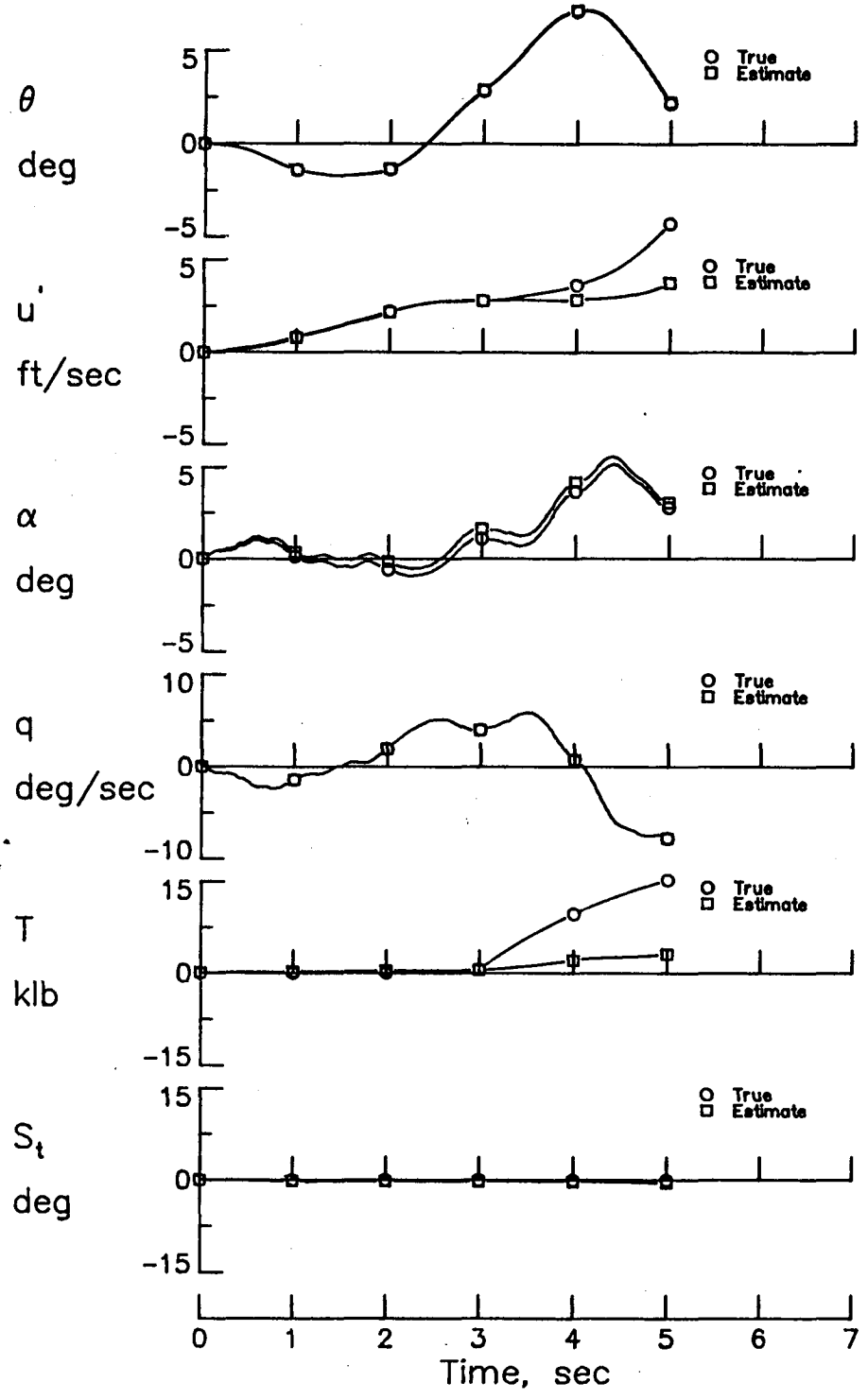

(a) Aircraft states.

Figure 6.- Constrained GLR results with heavy turbulence and -40° throttle failure at 3 seconds.

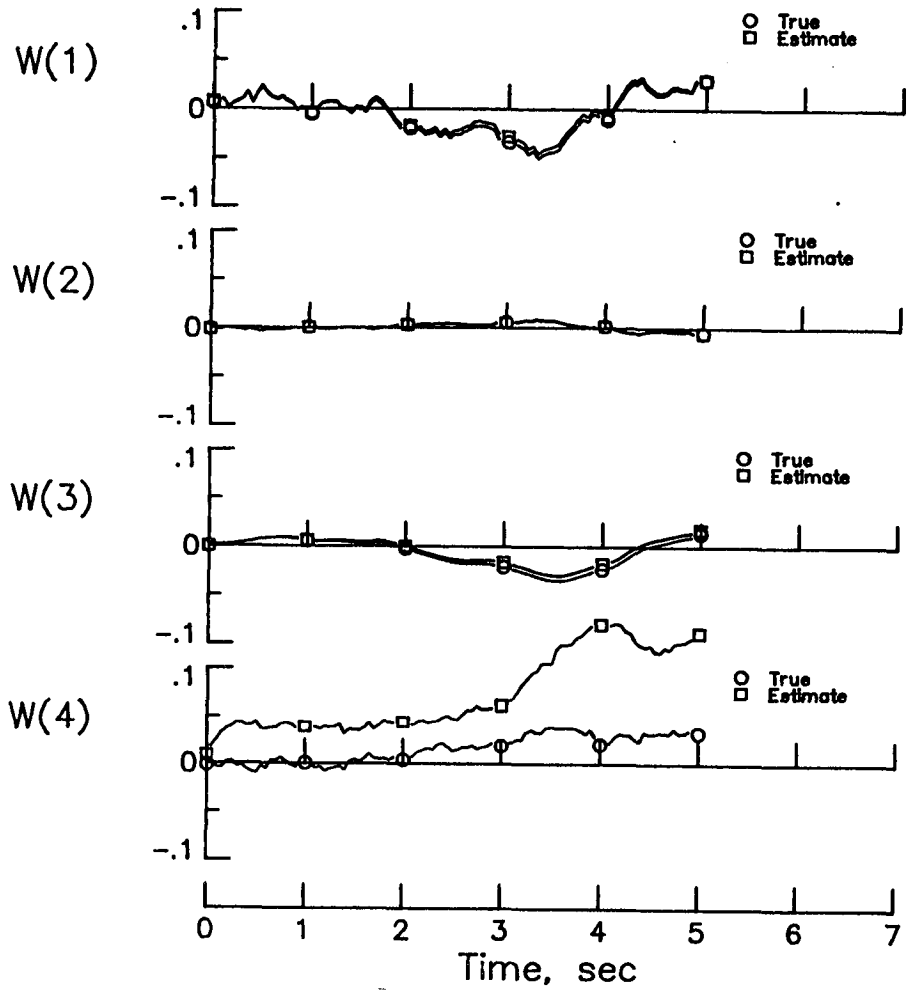

(b) Wind states.

Figure 6.- Continued.

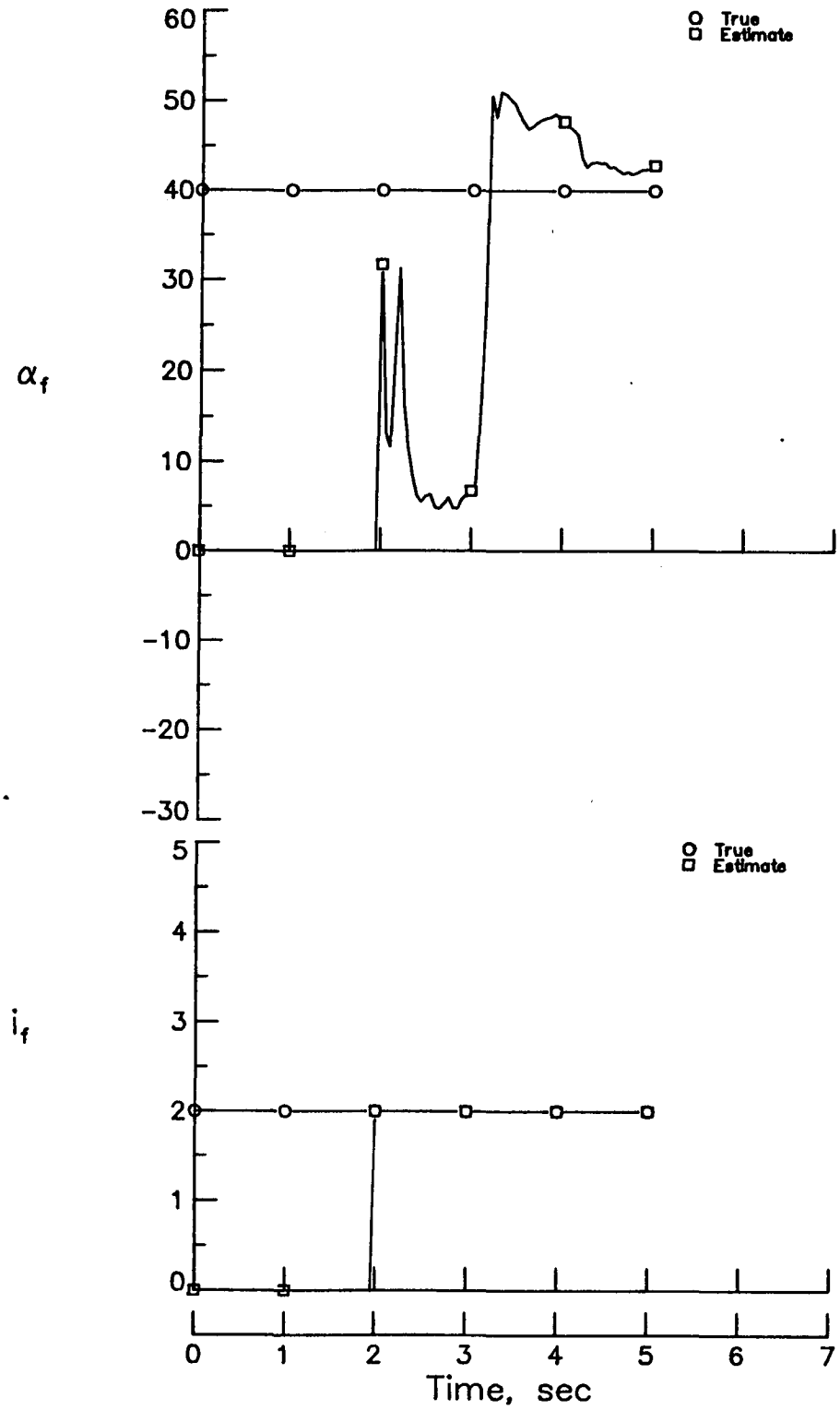

(c) Failure parameters.

Figure 6.- Continued.

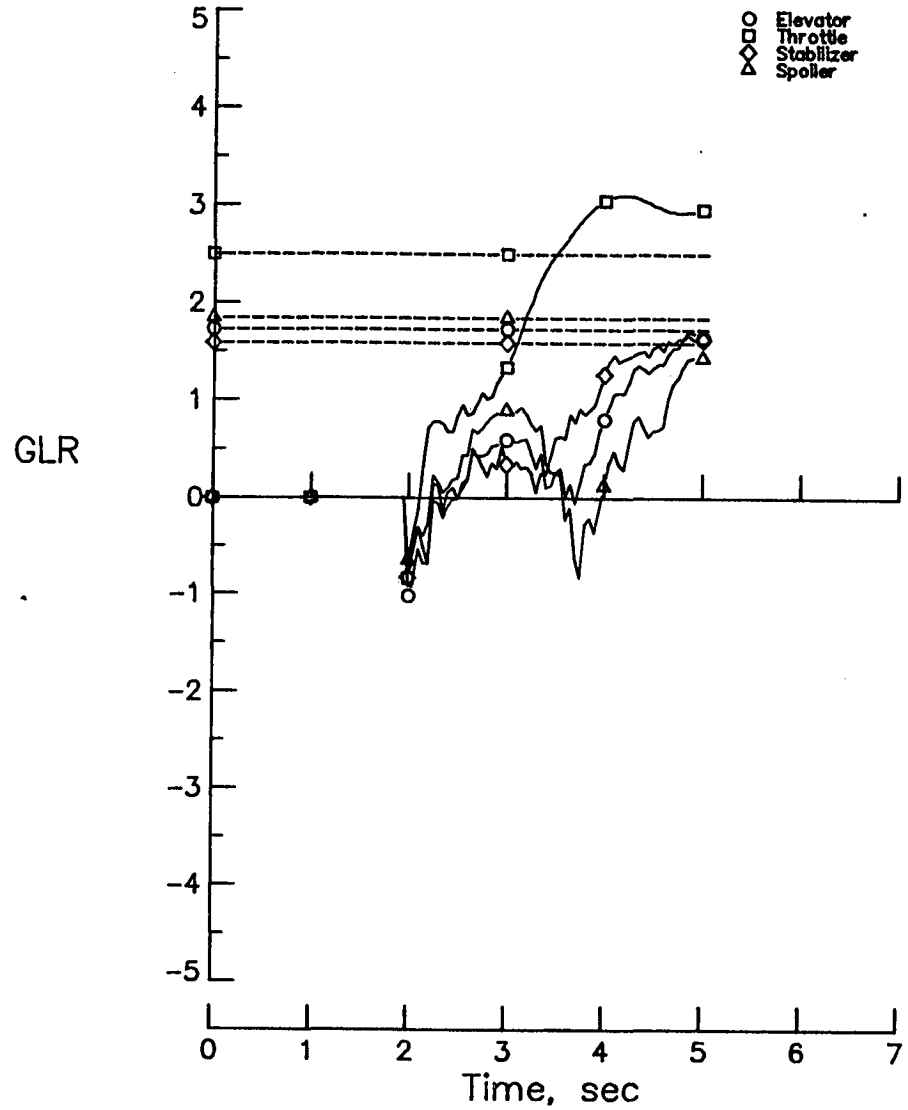

(d) Generalized likelihood ratios.

Figure 6.- Concluded.

1. Report No.	2. Government Accession No.	3. Recipient's Catalog No.
NASA TM-87620		

4. Title and Subtitle : A Preliminary Evaluation of the Generalized Likelihood Ratio for Detecting and Identifying Control Element Failures In A Transport Aircraft	5. Report Date: September 1985 6. Performing Organization Code: 505-34-03-07
7. Author(s): W. Thomas Bundick	8. Performing Organization Report No. 10. Work Unit No.
9. Performing Organization Name and Address: NASA/Langley Research Center, Hampton, VA 23665	11. Contract or Grant No. 13. Type of Report and Period Covered: Technical Memorandum
12. Sponsoring Agency Name and Address: National Aeronautics and Space Administration, Washington, DC 20546	14. Sponsoring Agency Code

15. Supplementary Notes

Programming support was supplied by Mrs. Jessie Yeager of PRC-Kentron.

16. Abstract

The application of the Generalized Likelihood Ratio technique to the detection and identification of aircraft control element failures has been evaluated in a linear digital simulation of the longitudinal dynamics of a B-737 aircraft. Simulation results show that the technique has potential but that the effects of wind turbulence and Kalman Filter model errors are problems which must be overcome.

17. Key Words (Suggested by Author(s))	18. Distribution Statement
Failure Detection GLR Fault Detection Restructurable Likelihood Ratio	Unclassified - Unlimited Subject Category - 08

19. Security Classif. (of this report)	20. Security Classif. (of this page)	21. No. of Pages	22. Price
Unclassified	Unclassified	93	A05

For sale by the National Technical Information Service, Springfield, Virginia 22161